

Response to reviewer comments

Original reviewer comments are in *italicized text*.

Our replies are in plain text.

Bold text shows small corrections within the original text.

We (K. E. Clark and co-authors) are providing a revised version of our manuscript for consideration and would like to thank the two referees (anonymous referee #1 and Ken Ferrier) for their reviews, which we feel helped us to substantially improve our paper during revision. In particular, we now include an expanded methodological discussion and a table detailing the soil carbon stock data, in response to the request from both reviewers for more information about these calculations. We provide detailed responses to these and other comments below, and our revision incorporates our thorough effort to address each of these points.

Detailed response to interactive comment from reviewer #1 (anonymous)

In their paper “Storm-triggered landslides in the Peruvian Andes and implications for topography, carbon cycles, and biodiversity”, Clark et al. present a largely remote sensing-based investigation of landslide distribution in space and time. They draw on field-derived measurements of soil properties and carbon content to derive carbon yields. They draw a number of conclusions about the degree, timing, and distribution of erosion and carbon export in the Kosñipata valley. This is a well-conceived and well supported study that has incremental, but important, implications for geomorphic studies. In particular, the authors make some very good points about landslide inventory biases by spatial-temporal variability, and the possible control on biomarkers.

We thank the reviewer for these positive comments on our paper.

General comments:

More information is needed around the calculation of soil organic carbon. A table in the supplemental data would be appreciated here. Is a single density used for each pit? Seeing the depth intervals and carbon/density values would help the reader to understand why the calculated carbon stocks here are 2x (give or take, according to Figure 7a) the previous estimates. I would like to see an explanation of why these values are higher, not just that this dataset is more complete.

Reviewer #2 raised a similar concern, and we appreciate both reviewers making the point that the manuscript needed more background information about the soil pits and associated soil carbon stock calculations. As suggested by the reviewer, we now include a supplementary table (Table S3) that describes the location of plots, forest type, number of pits dug per plot, average depth of plot and average soil carbon stock. In addition, in the revised main text (section 3.3) we have clarified the calculation of soil organic carbon content, as follows:

“Carbon stocks were determined by multiplying interval depth (m) and measured soil organic carbon content (%) by bulk density (g cm^{-3}) **for each soil layer. %OC was measured in each layer for every pit. For each plot one pit was measured for bulk**

density at the following intervals: 0-5, 5-10, 10-20, 20-30, 30-50, 50-100, 100-150 cm, and the depth-density trend from this pit was applied to other pits from the same plot. Soils were collected and processed following the methods Quesada et al. (2010). An average SOC stock (in tC km⁻²) for each plot was determined from the mean of individual pit SOC stocks (Fig. 7a; Table S3).

The reviewer also asked for more complete consideration of why the soil OC values are higher in this study than reported in previous papers. In our original Discussions paper, we attributed these differences primarily to the different depths over which C stocks are integrated (prior studies calculated stocks over only the top 30 or 50 cm, while we calculate over the full depth of mobile soil material, varying by plot from average depths of 33 to 158 cm, as now reported in Table S3). The reviewer's comment stimulated us to consider the comparison to prior work in more detail. We do not have access to the original data from prior studies (only the final C stock values), so we cannot provide detailed comparison of depth-by-depth C concentrations, as suggested by the reviewer. However, we can calculate an inferred C stock for the pits reported in our study over the top 0-30 cm and 0-50 cm intervals, matching the depth intervals used in prior work. The resulting values are similar to those reported in the prior respective studies, lending confidence to our interpretation and emphasizing that the differences can be attributed primarily to integration depth. We have included this new comparative analysis in new figure in the supplement (Figure S2) and we discuss this comparison in more detail in Section 3.3.2, as follows (all new text):

“Our soil C stock values are a factor of 1.2 to 1.7 higher than values reported in these previous studies (Girardin et al., 2014a; Zimmermann et al., 2009). For the same soil pit data (i.e., density and %C) used in this study, calculation of soil C stocks over depths equivalent to those used in the prior studies (i.e., over the top 0-30 cm and 0-50 cm) yields values in close agreement with those previously reported (Fig. S2). This consistency indicates that the differences between the full-depth values used here, versus the partial depth values reported previously, are attributable predominantly to the integration depth used.”

The mapped landslides include both scars and deposits. Please discuss the implications beyond the inclusion of low slopes. This would make some, but possibly not all, landslide areas too large. Might there be a topographic bias associated with this?

We have expanded our consideration of the implications of mapping landslide scars and deposits together, pointing out that this approach should still capture the extent of landslide effects on biomass. We have added the following paragraph to Section 3.1, in the Methods (all new text):

“The landslide areas visible via spectral contrast in the Landsat images include the regions of failure, run-out areas, and deposits. In some of the high-resolution imagery, we were able to distinguish scars from deposits, but not systematically enough to separately categorize these for the full landslide catalogue in this study. One 2007 landslide was coupled to a particularly large debris flow and stood out within our inventory, with the 1.7 km long debris flow comprising ~5% of the total landslide area for the total inventory from 1988 to 2012. With

this one exception, we consider all areas with visible contrast outside of river channels as being “landslide” area (e.g., see Fig. 2a and inset photo). For the purposes of quantifying biomass disturbance and organic carbon fluxes associated with landslide activity, the convolution of scars and deposits is justified on the basis that all of these areas were covered in forest prior to landslide occurrence. However, the fate of carbon from scars vs. deposits may differ, as discussed below, and when considering the slope distribution of landslide areas, the role of deposit areas introduces some bias (see further discussion in Section 4.2, below). Future landslide mapping work, taking advantage of even higher resolution imagery than available in this study, would benefit from the effort to explicitly distinguish scars and deposits for full inventories.”

As suggested by the reviewer, we have also clarified the potential implications for the relation between landslide occurrence and topography, with the following text added to Section 4.2 (all new text):

“Since our mapping did not distinguish landslide scars from deposits (see Section 3.1), systematic changes in the ratio of scar to deposit area with elevation could influence apparent patterns of landslide occurrence. For example, larger deposit areas at low elevation would increase calculated susceptibility even if the total landslide scar area were not larger. However, our anecdotal field observations do not suggest that landslides at lower elevations have consistently longer run-out or larger deposit areas, so it is unlikely that such bias explains the observed relations between landslide occurrence and topography within our inventory.”

The relationship between erosion and topography is not clear. Based on the landslide inventories, the authors suggest that erosion rates are highest at low elevations and decrease with elevation. They also state that the low elevation plateau may be a result of high erosion rates not yet propagating onto the plateau. Based on their mapping, the knickpoints in the streams representing this boundary occur at ~1400-1600 m a.s.l. The landslide-derived erosion rates peak at least 1000 meters higher. I understand that part of the paper shows the importance of the single event, but it seems that something is missing from the discussion.

Landslide susceptibility, which is the relevant metric for describing the extent of landslide-associated erosion, increases below the elevation range around 1500-2000m (Fig. 5b), which is coincident with the observed fluvial knickzone, at least within our ability to resolve this zone. These two features are not offset by 1000 m, as the reviewer states. The reviewer may be referring to Fig. 5a, which shows total landslide area as a function of elevation, which does indeed peak at elevations around 3000 m. But the catchment area at these elevations is much larger, so the effective depth of erosion associated with landslides is lower (as reflected in the landslide susceptibility in Fig. 5b). We apologize that this distinction was confusing in our original text and have revised Section 5.2.2 in an effort to clarify this aspect, as follows (mostly new text):

“A second set of information comes from the Kosñipata Valley topography and its relation to implied erosion associated with landslide activity. Although total landslide area in our Kosñipata dataset is greatest at mid-elevations, these mid-elevation landslides are distributed over a relatively large catchment area (Fig. 5a). Effective landslide erosion is greatest where landslide susceptibility on a unit-area basis is highest (Fig. 5b), so our inventory implies focused landslide erosion at lower elevations (< ~1500-2000 m) in the Kosñipata Valley, specifically associated with the 2010 storm (Figs. 2a, 5). This focused erosion appears to spatially coincide with the observed transition in the river channel profile at ~1700 m elevation, marked by the vertical step knickpoint (Fig. 10a).”

Specific comments:

pg. 637 – bottom: More landslides should result in lower concentration of cosmogenic nuclides in quartz. If sediment cosmogenic nuclide-derived erosion rates are lower than the landslide rates, then they have ‘higher’ concentrations than they should. This implies that there is either significantly storage of material (that does not make it into the river system), or that there is total bypass and poor mixing (i.e. cosmogenic nuclide-derived rates are local and not representative of catchments as a whole). This is not crucial to the paper, but it is an interesting topic.

We agree that the comparison of landslide and cosmogenic erosion rates is interesting, and the reviewer makes an insightful argument about some of the potential implications. Nonetheless, our paper is not focused on determining or interpreting cosmogenic erosion rates, so we view more detailed comparative analysis along these lines as beyond our present scope. We have modified the text to acknowledge the possibility for further work on this topic, particularly noting the potential for comparing the two sets of data collected from exactly the same catchment (which is not possible with current information). Our revised text reads as follows:

“The difference between the landslide-associated erosion rates measured in Bolivia (Blodgett and Isacks, 2007) and the catchment-averaged denudation rates typical of this region has not been widely considered, **and a more systematic comparison including data paired from identical catchments could offer fruitful avenues for further investigation. For the purposes of this study**, the observation of relatively high landslide rates suggests at the least that landslides are the primary mechanism of hillslope mass removal, as they are in other active mountain belts (Hovius et al., 2000; Hovius et al., 1997).”

Pg. 647 – middle: If the landslide inventory also includes depositional areas, then this is not a conservative estimate.

As noted above, areas associated with landslide deposits are also cleared of vegetation as a result of landslide activity, and we think this biomass should be included in the overall landscape-wide calculation of the amount of carbon stripped from hillslopes by landslides. We have added a note to clarify that the fate of carbon associated with landslide scars vs. deposits may differ, but that such differences are not well known (all new text):

“Calculated fluxes include carbon that was residing both on landslide scars and in areas of runout and deposit. The fate of carbon from each of these areas may differ, but such differences are not well known and we consider all to contribute to the loss of previously living biomass as a result of landslide occurrence.”

Pg. 647 – bottom: Why New Zealand? Give some justification for this comparison.

We have provided a comparison to data from Guatemala and New Zealand because these are the only studies to estimate landslide-associated carbon fluxes from montane systems over annual to decadal timescales, at least as far as we are aware. We have reworded the text to clarify that we are trying to make a general comparison:

“The area-normalized landslide carbon yield in the Kosñipata Valley is similar to the upper end of landslide carbon yields **for other mountain sites around the world where landslide carbon fluxes have been evaluated.**”

(Note also that we have moved this comparison to the Discussion, consolidating what was previously repetitive text).

Pg. 649 – middle: You might want to distinguish the ‘work done’ by landslides (which is removal of material here) from the geomorphic work done by landslides in the topographic sense (steep lower slopes).

The reviewer raises a good point. We have changed the text in section 5.1 to read:

“Here we define geomorphic work, *sensu* Wolman and Miller (1960), **as total landslide area, reflecting the removal of material from hillslopes (rather than, for example, the work done by landslides to modify slope angles).**”

Pg. 650 – lines 8-12: does not make sense.

We thank the reviewer for bringing this typo to our attention; we have changed “at” to “to”, as follows: “The notable shift from low **to** high landslide susceptibility above 30-40° (Fig. 6b) is consistent with the hillslope angles that reflect rock strength expected for the metamorphic and plutonic bedrock (Larsen and Montgomery, 2012).”

Pg 653 – top: this is too speculative. You could discuss the potential controls on topography, but should avoid discussions of erosion.

We have removed “erosion” from this sentence.

Detailed response to interactive comment from reviewer #2 (K. Ferrier)

We thank the reviewer, Ken Ferrier, for a thorough and positive review. We have modified

several aspects of the manuscript to cover the issues he raised.

General comments:

The central aim of this manuscript is to measure landslide-derived organic carbon fluxes out of the Kosñipata catchment in the eastern Andes. The authors computed these fluxes from the size of landslides, which they mapped using annual satellite images over the period 1988-2012, and the abundance of organic carbon in the material eroded by the landslides, which they estimated from new measurements of organic carbon stocks in soils and vegetation. These measurements took considerable effort: The authors analyzed a large number of satellite images and dug a large number of soil pits to estimate organic carbon stocks and fluxes. Their analysis implies that landslides in the Kosñipata basin have been responsible for large fluxes of organic carbon out of the catchment, with roughly three quarters of the flux coming from soil carbon and the rest from vegetation. These measurements are likely to be of interest because organic carbon fluxes from continents to the oceans are an important link in Earth's carbon cycle, and because the extent to which these fluxes are influenced by large erosional events is not well known. These new measurements are the manuscript's greatest strength.

We are pleased that the reviewer enjoyed the paper and appreciate his succinct summary of our analysis.

I have a few suggestions for strengthening the manuscript. Most importantly, I suggest adding an explanation for how the landslide-derived fluxes were calculated.

We have considerably revised Section 3.3 of the Methods, splitting this into three subsections. The first subsection comprises two new paragraphs that set out the methodological approach for determined landslide-derived carbon fluxes and put this approach within the context of prior related work (this text is not repeated in full here, for brevity, but is included in the manuscript showing tracked changes).

We have also revised the text of what is now Section 3.3.3, to help clarify how landslide-associated fluxes were calculated. We have also taken the opportunity to make a minor but important revision to these calculations. We now only quantify the above ground biomass, soil and below ground biomass, which dominate the carbon stock and show variability with elevation which can be described by a linear model with quantified uncertainties (see revised Fig. 7). This allows us to propagate the uncertainty on the elevation vs carbon stock models through the calculations which use landslide area to quantify carbon flux and carbon yield (e.g. see Table 2). We do not include the epiphytes and wood debris in this calculation because they make up a minor component of the carbon stock (<~10%) and their carbon stocks are not clearly linked to elevation. We instead provide an estimate for how much epiphytes and woody debris are likely to contribute in Section 4.4.

These revisions do not impact any of the conclusions of our study, and so do not impact the revised version in a major way. However, they do help strengthen our findings by providing a robust estimate of uncertainty to the carbon yields, which we include throughout the main text.

At present, the organic carbon fluxes are reported in section 4.4 without an explanation

for how they were calculated. An important aspect of this is landslide thickness: How did the authors estimate the thickness of eroded material in each of the landslides? Landslide thickness is required to estimate the mass of soil eroded in each landslide, which in turn is required to compute the organic carbon flux as the mass of the eroded soil multiplied by the organic carbon concentration in the soil.

The reviewer raises an important point about the relevance of landslide thickness to the calculated carbon fluxes. We mentioned briefly in our original Discussions paper that we assume all landslides strip the full soil depth, but we agree that this aspect could have been better developed. Previously we justified this assumption on the basis of field observations that most Kosñipata landslides clear soil to bedrock. We have now added an analysis based in geometric scaling relationships for landslides. This analysis indicates that the vast majority of landslides in our inventory are deeper than the deepest observed soils (covering >98% of landslide area, and maybe more), supporting our inferences from field observations.

We have added a new paragraph to the end of Section 3.3.3 discussing the importance of landslide thickness, as follows (all new text):

“In our calculation, landslides are assumed to strip all above ground and root biomass from hillslopes, based on field observations from the Kosñipata Valley that landslides are cleared of visible vegetation and roots. We also assumed landslides completely remove soil material to full depth, again consistent with field observations that landslides in the Kosñipata catchment are typically bedrock failures that remove the entire mobile soil layer. To test this latter assumption, we used geometric scaling relationships for landslides in mountainous terrain (Larsen et al., 2010) to estimate landslide depths. We calculated landslide volume from the area (A)-volume (V) relationship, $V = \alpha A^\gamma$ where α and γ are scaling parameters (we used $\alpha = 0.146$ and $\gamma = 1.332$, from the compilation of global landslides in Larsen et al., 2010, but also tested other literature values). We estimated depth by dividing volume for each landslide by the respective landslide area.”

And in Section 4.4, we now describe the results of this additional analysis:

“On the other hand, our values may overestimate fluxes from soil OC if landslides are shallower than soil depths, since we have assumed complete stripping of soil material to full soil depth and since soil OC stocks depend on depth of integration (see Section 3.3, above). Using the average scaling parameters for global landslides (Larsen et al., 2010), the minimum landslide depth in our inventory would be 0.74 m. Average soil depths at most plots were deeper, with the deepest being 1.58 m. However, for the same scaling parameters, only 99 landslides in our inventory, equating to 0.06 km² total landslide area (or ~2% of total landslide area), would be shallower than deepest soils at 1.58 m. Using scaling parameters for bedrock landslides only ($\alpha = 0.146$ and $\gamma = 1.332$; Larsen et al., 2010), yields only one landslide shallower than 1.58 m. This analysis corroborates our field observations that most landslides in the Kosñipata Valley clear soil and expose bedrock. We thus view our calculation of fluxes on the basis of complete stripping of soil as providing a reasonable estimate.”

Additional text that describes this would also provide a basis for reporting uncertainties on the organic carbon stocks and fluxes, which the manuscript currently lacks and would benefit from.

We have now included an uncertainty analysis, propagating errors on the elevation trends in OC stocks through to the calculation of landslide-associated carbon yields and fluxes (see reply to earlier comment). These uncertainties are reported in the revised section 4.4 and in table 2. As noted above, we also now report in Section 4.4 a lower bound on carbon fluxes based on assuming shallow landslide depths.

In addition, I suggest adding a section that describes the connectivity of the mapped landslides to the channel network. What fraction of the landslide-mobilized material made it to the channel network? This connectivity can vary substantially among regions. The authors briefly mention this issue in other studies on p. 656, but the manuscript does not explain how they estimated what fraction of the landslide material actually reached the channel network.

We thank the reviewer for this suggestion. In section 5.4 of the revised text, we now discuss landslide-river connectivity in the study area, as follows (all new text):

“The extent to which landslides connect to river channels exerts a first-order control on the fate of landslide material (Dadson et al., 2004), and thus on the fate of carbon. We identified landslides as connected or unconnected to rivers by manually inspecting high-resolution imagery and following landslides to their termination (i.e. to their lowest elevation point). Connected landslides terminated in river channels, identifiable by the absence of vegetation. We found that, for the Kosñipata Valley during our study period, greater than 90% of landslides were directly connected with rivers, similar to the high connectivity found for other storm-triggered landslides (e.g., West et al., 2011). However, even with high connectivity, it remains uncertain in the case of the Kosñipata how much of the material stripped by landslides is actually removed by rivers and exported out of the valley.”

Lastly, it would be useful to provide more descriptions of the soil pits, perhaps in the supplementary material. Specifically, it would be useful to see maps that show where the soil pits were dug, and profiles on organic carbon concentrations in each pit. These would put the calculations of organic carbon fluxes in context, by showing how representative the soil pits are likely to be of the catchment as a whole.

Reviewer #1 raised a similar point. In response, we have included a table of the soil plot data used in this study (Table S3), providing the location of the plots and associated carbon stocks. This reviewer also suggested including maps of soil pit locations and profiles for each pit. Although we agree that such further analysis would be interesting, we view it as outside the scope of this already lengthy manuscript, and as likely target for future manuscripts from co-

authors, considering in more detail the patterns of variability in soil OC within and across the plots.

In summary, this manuscript presents some new estimates of landslide-derived organic carbon fluxes based on an extensive series of new measurements. I believe that the manuscript would be strengthened by considering the issues I listed above, which I believe the authors could address in a moderately revised version of the manuscript. Below I list more a few more suggestions for improving the manuscript.

We hope the reviewer agrees that our changes have addressed his comments and strengthened the manuscript in the process.

Specific comments:

p. 633, lines 10-11: This states that “landslides may completely turnover hillslopes every ~1320 years”. This is strictly true only if landslides occur in every part of the catchment (do they?), and if landslides do not recur in the same place until the entire catchment has been resurfaced. By Figure 2 it looks as if some portions of the catchment did not experience any landslides during the observation period. I’d suggest rephrasing this slightly to reflect that.

We have rephrased the abstract to address this important point:

“Catchment-wide landslide rates were high, at 0.076% yr⁻¹ by area. As a result, landslides **on average** completely turn over hillslopes every ~1320 years, **although our data suggest that patterns of landslide occurrence varies spatially, such that turnover times are likely to be non-uniform**. In total, landslides strip 26±4 tC km⁻² yr⁻¹ of soil (80%) and vegetation (20%).”

p. 636, line 11: What does spp stand for in the units for species richness? I suggest defining that here.

spp stands for species, a term we use in full in the revision.

p. 641, lines 23-25: It would be useful to specify in the text not only that the carbon stocks estimated in the present study differ from those in previous studies, but also to state that these estimates are bigger, and to quantify how much bigger.

In response also to comments from Reviewer #1, we have re-written this section and now include a quantitative comparison, now stating that, “Our soil C stock values are a factor of 1.2 to 1.7 higher than values reported in these previous studies (Girardin et al., 2014a; Zimmermann et al., 2009).”

p. 644, line 8: It would be appropriate to cite some older papers here, especially Zhang and Montgomery, 1994, Water Resources Research, v. 30, p. 1019-1028.

We thank the reviewer for suggesting this additional reference and have added it to the text in section 3.5.

p. 647, lines 2-3: Is this a lot of carbon or a little? I suggest providing context for these numbers here by comparing them to carbon stocks in other places. Also: What are the uncertainties on these values? That would be a valuable quantity to report for the carbon stocks (and for other quantities too), because it'll aid comparisons to future studies.

We now include the follow sentence which qualifies how these soil and vegetation stocks compare broadly with other ecosystems:

“Overall, the vegetation carbon stock values from the Kosñipata Valley are slightly lower than lowland tropical forests, and the soil values higher (Dixon et al., 1994), which is consistent with broad trends in the tropics in which soil carbon stocks increase with elevation and are frequently greater than vegetation carbon stocks (Gibbon et al., 2010; Raich et al., 2006).”

We have also incorporated an uncertainty analysis through error propagation and it is included in the revised manuscript in section 4.4. We have addressed his comments on error in the general comments section.

p. 647, lines 7-11: These fluxes are likely to be conservative because they implicitly assume that landslides are the only means of conveying organic carbon to the channels. How much carbon is eroded to the channel network by other processes (e.g., soil creep)?

Total erosion rates are not yet known for our study site, so we are not able to quantify rates of soil creep and other erosional processes. However, we agree that these may also be relevant mechanisms of transporting carbon and have now added a sentence to the end of Section 4.4 that brings this additional process to readers' attention (all new text):

“When considering carbon budgets at the landscape-scale, the landslide-associated carbon fluxes we report here should also be viewed in the context that other processes such as soil creep may additionally contribute to the transfer of carbon from hillslopes to rivers (e.g., Yoo et al., 2005).”

p. 648, lines 13-14: I was a little confused by the wording in this sentence. Instead of writing “where RI_i is the return time for a year characterized by the landslide magnitude of year i ”, I suggest replacing it with something like, “where RI_i is the return interval for the i th largest landslide in the record.”

We thank the reviewer for pointing out this confusing explanation in our Discussion paper. We have modified the text in section 5.1 of the revised manuscript, although we were concerned that the reviewer's specific suggested wording could be misleading. Instead, we now state: "where RI_i is the return **interval for the year with the i^{th} largest total annual landslide area.**"

p. 650, line 11: Angle of repose pertains strictly to granular material, so I'd suggest replacing "angle of repose" with something like "hillslope angles consistent with the strength of the local bedrock."

The reviewer makes a good point. We have modified the text in section 5.2.1 as suggested by the reviewer, though we preferred wording as follows: "The notable shift from low to high landslide susceptibility above 30-40° (Fig. 6b) **is consistent with the hillslope angles that reflect rock strength expected for** the metamorphic and plutonic bedrock (Larsen and Montgomery, 2012)."

p. 661, line 10: For the editors: the doi link appears to be broken.

We thank the reviewer for bringing this to our attention and will double-check the doi links in the final publication PDF.

p. 686, Figure 11: This is a busy figure, and the individual panels are quite small, which makes them difficult to read. Could this be split into multiple figures? Also: What is shown in panel c? The caption's only description of panel c is a reference to Figure 10, but it would be more helpful to state what it is directly here.

We apologise that the individual panels of figure 11 were difficult to read in the Discussion paper. We intend for this figure to be printed in a horizontal layout for final publication, which we hope will address this issue. Although we agree it remains a busy figure, the correspondence between the location of the fluvial transitions in (a-c) and the geology, precipitation, and cloud frequency is directly related to the interpretation, and we therefore prefer not to divide the panels into separate figures.

We have revised the caption to clarify the description of panel c, as follows: "Figure 11: (a-c) Analysis of river profiles analogous to those in Fig. 10 (shown here as River #3, in cyan), for rivers throughout the Alto Madre de Dios region (d). In (b), data are binned by upstream area and means are shown by black circles. Arrows in (a) refer to locations along the profile of observed transition in the area-slope plots (b). **In (c), hillslope angles (from STRM DEM) are separated between regions upstream (blue) and downstream (red) of the transitions.** Transition locations are displayed as red dots in (d-g), which show regional elevation (Farr et al., 2007) (d), geology (INGEMMET, 2013) (e), TRMM 2B31 annual precipitation (Bookhagen, 2013) (f), and Modis cloud frequency (Halladay et al., 2012) (g)."

1 **Storm-triggered landslides in the Peruvian Andes and implications for topography,**
2 **carbon cycles, and biodiversity**

3 Kathryn E. Clark^{1*}, A. Joshua West², Robert G. Hilton³, Gregory P. Asner⁴, Carlos A.
4 Quesada⁵, Miles R. Silman⁶, Sassan S. Saatchi⁷, William Farfan-Rios⁶, Roberta E. Martin⁴,
5 Aline B. Horwath⁸, Kate Halladay¹, Mark New^{1,9} and Yadvinder Malhi¹

6 ¹ Environmental Change Institute, School of Geography and the Environment, University of
7 Oxford, Oxford, UK.

8 (*correspondance: kathryn.clark23@gmail.com; Current address: Department of Earth and
9 Environmental Science, University of Pennsylvania, Philadelphia, PA, USA)

10 ² Department of Earth Sciences, University of Southern California, Los Angeles, CA, USA.

11 ³ Department of Geography, Durham University, Durham, UK.

12 ⁴ Department of Global Ecology, Carnegie Institution for Science, Stanford, CA, USA.

13 ⁵ Instituto Nacional de Pesquisas da Amazônia, Manaus, Brazil.

14 ⁶ Department of Biology and Center for Energy, Environment, and Sustainability, Wake
15 Forest University, Winston-Salem, NC, USA.

16 ⁷ Jet Propulsion Laboratory, California Institute of Technology, Pasadena, CA, USA.

17 ⁸ Department of Plant Sciences, University of Cambridge, Cambridge, UK.

18 ⁹ African Climate and Development Initiative, University of Cape Town, Rondebosch, Cape
19 Town, South Africa.

20 Abstract

21 In this study, we assess the geomorphic role of a rare, large-magnitude landslide-triggering event and
22 consider its effect on mountain forest ecosystems and the erosion of organic carbon in an Andean
23 river catchment. Proximal triggers such as large rain storms are known to cause large numbers of
24 landslides, but the relative effects of such low-frequency, high-magnitude events are not well known
25 in the context of more regular, smaller events. We develop a 25-year duration, annual-resolution
26 landslide inventory by mapping landslide occurrence in the Kosñipata Valley, Peru, from 1988 to
27 2012 using Landsat, Quickbird and Worldview satellite images. Catchment-wide landslide rates were
28 high, at 0.076% yr⁻¹ by area. As a result, landslides on average completely turn over hillslopes every
29 ~1320 years, although our data suggest that landslide occurrence varies spatially, such that turnover
30 times are likely to be non-uniform. In total, landslides stripped 26±4 tC km⁻² yr⁻¹ of organic carbon
31 from soil (80%) and vegetation (20%) during the study period. A single rain storm in March 2010
32 accounted for 27% of all landslide area observed during the 25-year study and accounted for 26% of
33 the landslide-associated organic carbon flux. An approximately linear magnitude-frequency
34 relationship for annual landslide areas suggests that large storms contribute an equivalent landslide
35 failure area to the sum of smaller frequency landslides events occurring over the same period.
36 However, the spatial distribution of landslides associated with the 2010 storm is distinct. On the basis
37 of precipitation statistics and landscape morphology, we hypothesize that focusing of storm-triggered
38 landslide erosion at lower elevations in the Kosñipata catchment may be characteristic of longer-term
39 patterns. These patterns may have implications for the source and composition of sediments and
40 organic material supplied to river systems of the Amazon basin, and, through focusing of regular
41 ecological disturbance, for the species composition of forested ecosystems in the region.

42 1. Introduction

43 | Landslides [are](#) major agents of topographic evolution (e.g., (Li et al., 2014; Egholm et al., 2013;
44 | Ekström and Stark, 2013; Larsen and Montgomery, 2012; Roering et al., 2005; Hovius et al., 1997)
45 | and are increasingly recognized for their important biogeochemical and ecological role in
46 | mountainous environments because they drive erosion of carbon and nutrients (Pepin et al., 2013;
47 | Ramos Scharrón et al., 2012; Hilton et al., 2011; West et al., 2011; Stallard, 1985) and introduce
48 | regular cycles of disturbance to ecosystems (Restrepo et al., 2009; Bussmann et al., 2008). Landslides
49 | result when slope angles reach a failure threshold (Burbank et al., 1996; Schmidt and Montgomery,
50 | 1995; Selby, 1993), which is thought to occur in mountains as rivers incise their channels, leaving
51 | steepened hillslopes (Montgomery, 2001; Gilbert, 1877). [Landsliding acts to](#) prevent progressive
52 | steepening beyond [a critical failure angle for](#) bedrock, even as rivers continue to cut downwards
53 | (Larsen and Montgomery, 2012; Montgomery and Brandon, 2002; Burbank et al., 1996). However,
54 | many slopes prone to landslide failure may remain stable until a proximal triggering event, such as a
55 | storm (Lin et al., 2008; Meunier et al., 2008; Restrepo et al., 2003; Densmore and Hovius, 2000) [or a](#)
56 | large earthquake (Li et al., 2014; Dadson et al., 2004; Keefer, 1994). [Intense storms can increase pore](#)
57 | [pressure from heavy rainfall \(Terzaghi, 1951\), decreasing](#) soil shear strength and [resulting in](#) slope
58 | failure (Wang and Sassa, 2003).

59 | By clearing whole sections of forest and transporting materials downslope, landslides can drive fluxes
60 | of organic carbon from the biosphere (Hilton et al., 2011; West et al., 2011; Restrepo and Alvarez,
61 | 2006), delivering the carbon either into sediments (where recently photosynthesized carbon can be
62 | locked away) or into the atmosphere, if ancient organic material in bedrock or soils is exposed and
63 | oxidized (Hilton et al., 2014). Links between storm frequency, landslide occurrence, and carbon
64 | fluxes could generate erosion-carbon cycle-climate feedbacks (West et al., 2011; Hilton et al., 2008a).
65 | Moreover, storm-triggered landslides may [link](#) climate [to](#) forest disturbance, with implications for
66 | ecosystem dynamics (Restrepo et al., 2009). However, for storm-triggered landslides to keep
67 | occurring over prolonged periods of time, hillslopes must remain sufficiently steep, which typically
68 | occurs in mountains via sustained river incision. Incision is also climatically regulated (Ferrier et al.,
69 | 2013), providing a mechanism connecting storm activity, erosion, and topographic evolution (e.g.,
70 | (Bilderback et al., 2015), and further linking to organic carbon removal from hillslopes and ecological
71 | processes across landscapes.

72 | In this study, we mapped landslides in a mountainous catchment in the Andes of Peru over a 25-year
73 | period, including one year (2010) in which a large storm triggered a [numerous](#) [landslides](#). We
74 | quantify landslide rates on an annual basis and use comprehensive datasets on soil and above- and
75 | below-ground biomass to determine the amount of organic carbon stripped from hillslopes. We assess
76 | the relative landslide ‘work,’ in terms of total landslide area, done in different years to explore the

77 roles of varying magnitudes and frequencies of triggering events, providing a longer-term context for
78 understanding storm-triggered landslides that has not been available in much of the prior research on
79 storm effects. We also evaluate the spatial distribution of landslides with respect to catchment
80 topography and climatic factors that may act as potential longer-term forcing on the location of most
81 active landslide erosion. Finally, we assess the potential role of these spatial patterns in shaping
82 regional topography, determining the composition of sediment delivered to rivers, and influencing
83 forest ecosystems that are repeatedly disturbed by landslide occurrence.

84

85 2. Study area

86 The Kosñipata River (Fig. 1) is situated in the Eastern Andes of Peru. We focus on the catchment area
87 upstream of a point (13°3'27"S 71°32'40"W) just downriver of San Pedro. Elevation in the catchment
88 ranges from 1200 metres above sea level (m) to 4000 m, with a mean elevation (± 1 standard
89 deviation) of 2700 ± 600 m and a catchment area of 185 km². The forested area covers 150 km² and
90 consists of tropical montane cloud forest at high elevations and sub-montane tropical rainforest at
91 lower elevations (Fig. 1a) (Horwath, 2011). The area of puna grasslands covers 35 km² above the
92 timberline at 3300 \pm 250 m range. The valley is partially contained in Manu National Park, where
93 logging is prohibited. A single unpaved road is located in the valley stretching from high to low
94 elevations. The Kosñipata River flows through the study area and into the Alto Madre de Dios River,
95 which feeds the Madre de Dios River, a tributary of the Amazon River. There are extensive datasets
96 on plants, soil, ecosystem productivity, carbon and nutrient cycling and climate within the catchment
97 (Malhi et al., 2010). Tree species richness ranges from 40 to 180 species ha⁻¹ for trees ≥ 10 cm diameter
98 at breast height (dbh), and total forest C-stocks (Gurdak et al., 2014; Girardin et al., 2013; Horwath,
99 2011; Gibbon et al., 2010) are representative of the wider Andean region (Saatchi et al., 2011).

100 The South American Low Level Jet carries humid winds westward over the Amazon Basin and then
101 south along the flank of the Andes, driving orographic rainfall in the Eastern Cordillera of the Central
102 Andes (Espinoza et al., 2015; Lowman and Barros, 2014; Marengo et al., 2004). In the study area,
103 precipitation ranges from 2000 to 5000 mm yr⁻¹ and is highest at the lowest elevations, decreasing
104 approximately linearly with the increase in elevation (Clark et al., 2014; Girardin et al., 2014b;
105 Huaraca Huasco et al., 2014). Much of the valley has >75% cloud cover throughout the year in a band
106 of persistent cloud that spans much of the Eastern Andes, although cloud immersion is restricted to
107 elevations $> \sim 1600$ m (Halladay et al., 2012) (Fig. 1a).

108 The Kosñipata Valley is in the tectonically active setting of the uplifting Eastern Cordillera of the
109 Central Andes, associated with subduction of the Nazca Plate under the South American Plate
110 (Gregory-Wodzicki, 2000). Since 1978, there have been ~ 4 registered earthquakes larger than

111 magnitude $M=5$ within a distance of 65 km from the Kosñipata Valley (Fig. 1b; (USGS, 2013a;
112 Gregory-Wodzicki, 2000)), though significant ground shaking within the Kosñipata Valley has not
113 | been reported during the [study](#) interval. The Cusco fault zone is the nearest seismically active region,
114 ~50 km southwest of the study site, consisting of normal faults stretching 200 km long and 15 km
115 wide parallel to the Andean plateau (Cabrera et al., 1991) and where deep earthquakes are common
116 (USGS, 2013a; Tavera and Buforn, 2001). In the Andean foothills, ~20 km northeast of the study site,
117 there is an active fold and thrust belt (Vargas Vilchez and Hipolito Romero, 1998; Sébrier et al.,
118 1985). The bedrock geology in the Kosñipata Valley is representative of the wider Eastern Andes
119 (Clark et al., 2013). The catchment is dominated by metamorphosed sedimentary rocks in the high
120 elevations (mostly mudstone protoliths of ~450 Ma) and a plutonic region in the lower elevations
121 (Carlotto Caillaux et al., 1996) (Fig. 1b).

122 Landslides are a pervasive feature of the landscape in the Kosñipata Valley. In general in the Andes,
123 landslides are a common geomorphic process, with landslide area covering 1-6% of mountain
124 catchments in parts of Ecuador and Bolivia (Blodgett and Isacks, 2007; Stoyan, 2000), and landslide-
125 associated denudation rates have been estimated in the range of 9 ± 5 mm yr⁻¹ (Blodgett and Isacks,
126 | 2007). [Downstream of the Kosñipata River](#), detrital cosmogenic nuclide concentrations in river
127 sediments in the Madre de Dios River suggest a denudation rate of ~0.3 mm yr⁻¹ (Wittmann et al.,
128 2009), although this catchment includes a large lowland floodplain area. Cosmogenic-derived total
129 denudation rates in the high Bolivian Andes range up to ~1.3 mm yr⁻¹ (Safran et al., 2005) and
130 suspended sediment derived erosion rates up to 1.2 mm yr⁻¹ (Pepin et al., 2013). The difference
131 between the landslide-associated erosion rates measured in Bolivia (Blodgett and Isacks, 2007) and
132 | the catchment-averaged denudation rates typical of this region has not been widely considered, [and a](#)
133 [more systematic comparison including data paired from identical catchments could offer fruitful](#)
134 [avenues for further investigation. For purposes of this study](#), the observation [of relatively high](#)
135 landslide rates suggests at the least that landslides are the primary mechanism of hillslope mass
136 removal, as they are in other active mountain belts (Hovius et al., 2000; Hovius et al., 1997).

137

138 **3. Materials and methods**

139 **3.1. Landslide mapping**

140 Landslides within the Kosñipata Valley were manually mapped over a 25-year period from 1988 to
141 2012 using Landsat 5 (Landsat Thematic Mapper) and Landsat 7 (Landsat Enhanced Thematic
142 Mapper Plus) satellite images (Fig. 2a) (USGS, 2013b). There were 38 usable Landsat images for the
143 region over the 25-year period, with 1-3 available for each year (see Supplement Table S1). All
144 images were acquired in the dry season (May-October). Landsat images were processed with a
145 Standard Terrain Correction (Level 1T) which consists of systematic radiometric and geometric

146 processing using ground control points and a digital elevation model (DEM) for ortho-georectification
147 (USGS, 2013b). The high frequency of the Landsat images made it possible to develop a time series
148 of individual landslides over the entire 25-year duration which has not typically been achieved before
149 in studies at the catchment-scale (Hilton et al., 2011; Hovius et al., 1997).

150 The landslide inventory was produced by manually mapping landslide scars and their deposits in
151 ArcGIS and by verifying via ground-truthing of scars in the field. Mapping involved visually
152 comparing images from one year to the next evaluating contrasting colour changes suggesting a
153 landslide had occurred. A composite image of Landsat bands 5 (near-infrared, 1.55-1.75 μm), 3
154 (visible red, 0.63-0.69 μm) and 7 (mid-infrared, 2.08-2.35 μm) was used in order to identify landslide
155 scars with the greatest spectral difference to forest. Bedrock outcrops are minimal in the valley and
156 thus not subject to mislabelling as landslides. Several aerial photographs (from 1963 and 1985) were
157 used to identify and remove pre-1988 landslides from this study.

158 The landslide areas visible via spectral contrast in the Landsat images include regions of failure, run-
159 out areas, and deposits. In some of the high-resolution imagery, we were able to distinguish scars
160 from deposits, but not systematically enough to separately categorize these for the full landslide
161 catalogue in this study. One 2007 landslide was coupled to a particularly large debris flow and stood
162 out within our inventory, with the 1.7 km long debris flow comprising ~5% of the total landslide area
163 for the total inventory from 1988 to 2012. With this one exception, we consider all areas with visible
164 contrast outside of river channels as being “landslide” area (e.g., see Fig. 2a and inset photo). For the
165 purposes of quantifying biomass disturbance and organic carbon fluxes associated with landslide
166 activity, the convolution of scars and deposits is justified on the basis that all of these areas were
167 covered in forest prior to landslide occurrence. However, the fate of carbon from scars vs. deposits
168 may differ, as discussed below, and when considering the slope distribution of landslide areas, the
169 deposit areas introduce some bias (see further discussion in Section 4.2, below). Future landslide
170 mapping work, taking advantage of even higher resolution imagery than available in this study, would
171 benefit from the effort to explicitly distinguish scars and deposits for full inventories.

172 The Landsat images had a mean visibility of 67% that varied year-to-year (Table S2; Fig. 3a). Non-
173 visible portions were due to topographic shadow, cloud shadow, and no-data strips on Landsat 7
174 images post-2002 (following failure of the satellite’s scan line corrector). Duplicate or triplicate
175 images were used in most years, and so landslides obscured by cloud shadow or no-data were likely to
176 be spotted within a year of their occurrence. Topographic shadow produced by hillslopes covered a
177 minimum of 21% of the study area (35 km² out of 185 km²), predominantly on southwest facing
178 slopes (223 \pm 52° azimuth), and was consistently present between images. Landslides that fell within
179 these shadow areas were not visible. Using Quickbird imagery from 2005 (which covers 54% of the
180 study area) we found that the Landsat topographic shadow areas have a similar area covered by

181 landslides as the visible areas; 26% of the Quickbird-mapped landslide area fell within Landsat
182 topographic shadow areas, and these areas encompass a similar 22% of the total image area. We thus
183 infer that landslide occurrence under Landsat topographic shadow is approximately equivalent to that
184 in the visible portion of the Landsat images. On this basis, we estimate an error of $< \sim 20\%$ in our
185 landslide inventory due to missed landslides under topographic shadow.

186 Small-area landslides are not fully accounted for by our mapping approach due to the Landsat grid-
187 resolution of 30 m x 30 m (Stark and Hovius, 2001). In addition, Landsat images may not allow
188 distinguishing of clumped landslides (cf. Marc and Hovius (2015); Li et al. (2014)). We assessed the
189 potential bias by comparing the Landsat imagery with Quickbird imagery from 2005 (at 2.4 m x 2.4 m
190 resolution). Specifically, we compared landslides mapped from portions of 2005 Quickbird image that
191 are visible in the Landsat imagery (i.e., not in topographic shadow, discussed above) with the
192 Landsat-derived landslides mapped from 1988 to 2005 that had not recovered by 2005. The difference
193 in landslide area is 181,760 m², equivalent to $\sim 25\%$ of the total landslide area. The area-frequency
194 relationships (cf. Malamud et al. (2004) and references therein) for the two datasets show similar
195 power law relationships for large landslides (Fig. 4) and illustrate that the different total landslide
196 areas can be attributed mainly to missing small landslides ($< 4,000$ m²) in the Landsat-derived maps.
197 These small landslides contribute $\sim 80\%$ of the observed difference, with the remaining difference
198 attributable to 3 larger landslides (total area 30,500 m²) missed due to other reasons such as image
199 quality. Based on the difference between total landslide area mapped via Quickbird vs. Landsat
200 imagery, we estimate an error of $\sim 20\%$ in our landslide inventory from missing small landslides and
201 $< 5\%$ error from missing larger landslides.

202 **3.2 Landslide rates, turnover times, and landslide susceptibility**

203 We calculated landslide rate (R_{ls} , % yr⁻¹) as the percentage of landslide area (A_{ls}) per unit catchment
204 area ($A_{catchment}$), i.e., $R_{ls} = 100 \times A_{ls}/A_{catchment} \times 1/25$ yr for all landslide area observed during the 25-
205 year study period. To assess the spatial distribution of landslides throughout the study area, we
206 determined rates by 1 km² grid cells (Fig. 2b).

207 The average rate of slope turnover due to landslides (t_{ls}) is the inverse of landslide rate. This metric
208 reflects the time required for landslides to impact all of the landscape, solely based on their rate of
209 occurrence (Hilton et al., 2011; Restrepo et al., 2009). t_{ls} was quantified over the visible portion of the
210 study area in 1 km² cells (Fig. 2c).

211 To assess how landslide rate varies with elevation and hillslope angle, we divided each landslide
212 polygon into 3 m x 3 m cells consistent with the Carnegie Airborne Observatory (CAO) digital
213 elevation model (DEM) (Asner et al., 2012) (see Appendix A). We used the resulting 3 m grid to
214 calculate histograms of landslide areas and total catchment area as a function elevation and slope
215 using 300 m and 1° intervals, respectively (Figs. 5, 6). We also defined landslide susceptibility (S_{ls})

216 for a given range of elevation or slope angle values, as the ratio of the number of landslide cells in
217 each elevation (or slope) range, divided by the total number of catchment cells in the equivalent
218 range. Consistent with the landslide rate analysis, we only used catchment cells in the portion of the
219 study area visible in the Landsat images.

220 **3.3. Calculation of carbon stripped from hillslopes by landslides**

221 **3.3.1. General approach to calculating landslide-associated carbon fluxes**

222 We seek to quantify the amount of organic carbon mobilised by landslides at the catchment scale.
223 This requires knowledge of the spatial distribution of carbon stocks on forested hillslopes at this scale.
224 One approach is to use forest inventory maps derived from field surveys, aerial imagery, or other
225 remote sensing observations (Asner et al., 2010; Saatchi et al., 2007) along with mapped landslides
226 (e.g., (Ramos Scharrón et al., 2012; West et al., 2011). However, such forest inventories do not
227 typically capture below-ground or soil carbon stocks, the latter of which can make up the majority of
228 total organic carbon in the landscape (Eswaran et al., 1993). Maps of soil C can be estimated from soil
229 surveys together with knowledge of the C content in each soil type (Ramos Scharrón et al., 2012), but
230 sufficiently detailed soil surveys are often unavailable and it is also difficult to test the key assumption
231 that C content is constant for a given soil type.

232 An alternative approach, which we adopt in this study, is to use empirical trends in C stocks as a
233 function of elevation, and to assign landslide area at a given elevation with a C stock value
234 representative of that elevation (Hilton et al., 2011). Scatter in the relationship between elevation and
235 C stocks (cf. Fig. 7, Table 1) means these trends do not provide the basis for a robust map of C stocks,
236 nor a precise value for any single individual landslide. However, landslides in a setting like the
237 Kosñipata Valley occur distributed across the catchment area at a given elevation, and the large
238 number of landslides effectively samples from the observed scatter in C stocks. This averaging means
239 that, when we sum together estimates of C stock stripped by all landslides across the catchment, we
240 can estimate a representative mean value for the total flux of landslide-associated carbon. An implicit
241 assumption is that there is not a systematic, coincident spatial bias in both landslide location and C
242 stock at a given elevation (e.g., see discussion of potential slope biases on C stock estimates, below).

243 **3.3.2. Carbon stocks as a function of elevation**

244 To constrain trends in C stocks with elevation in the Kosñipata catchment, we collated soil and
245 vegetation datasets, taking advantage of the numerous plot studies. The datasets consist of soil carbon
246 stocks, above ground living biomass (trees), and root carbon stocks (Girardin et al., 2010). Each
247 dataset consisted of data from 6 to 13 plots along the altitudinal gradient (Fig. 7). Linear regressions
248 of C stock (tC km⁻²) versus elevation (m) were determined for the soil, above ground living biomass,
249 and roots separately (Hilton et al., 2011) and are reported in Table 1. For above ground living

250 biomass, we assumed a wood carbon concentration of 46% measured in stems and leaves (n = 130)
251 throughout the Kosñipata Valley (Rao, 2011). The trend in above ground biomass versus elevation
252 from this dataset fits within the range reported by Asner et al. (2014). Additionally, data on wood
253 debris carbon stocks (Gurdak et al., 2014), and epiphyte carbon stocks (Horwath, 2011) are available
254 but were not used in the carbon stock analysis because: (i) these comprise a small proportion of the
255 total biomass (see below), and (ii) do not show systematic change with elevation, precluding the use
256 of our elevation-based approach for these biomass components.

257 For soil organic carbon (SOC) stocks, we used data from soil pits along the altitudinal gradient. Pits
258 were dug at 11 forest plots, each with 6 to 51 individual soil pits per plot. Soil pits were dug from the
259 surface at 0.05 to 0.5 m depth intervals until reaching bedrock, which was typically found at ~1 m
260 depth (see Supplement Table S3). Carbon stocks were determined by multiplying interval depth (m)
261 and measured soil organic carbon content (%OC) by bulk density (g cm^{-3}) for each soil layer. %OC
262 was measured at each layer for every pit. For each plot one pit was measured for bulk density at the
263 following intervals: 0-5, 5-10, 10-20, 20-30, 30-50, 50-100, 100-150 cm, and the depth-density trend
264 from this pit was applied to other pits from the same plot. Soils were collected and processed
265 following the methods Quesada et al. (2010). An average SOC stock (in tC km^{-2}) for each plot was
266 determined from the mean of individual pit SOC stocks (Fig. 7a; Table S3).

267 Compared to previously published SOC data for this region, this dataset is the most complete,
268 encompassing more pits per plot and considering the full soil depth. Prior studies have considered the
269 SOC stock over a uniform 0-30 cm depth (e.g., (Girardin et al., 2014a) or considering separate
270 horizons to a depth of 50 cm (Zimmermann et al., 2009). Our soil C stock values are a factor of 1.2 to
271 1.7 higher than values reported in these previous studies (Girardin et al., 2014a; Zimmermann et al.,
272 2009). For the same soil pit data (i.e., density and %C) used in this study, calculation of soil C stocks
273 over depths equivalent to those used in the prior studies (i.e., over the top 0-30 cm and 0-50 cm)
274 yields values in close agreement with those previously reported (see Supplement Fig. S1). This
275 consistency indicates that the differences between the full-depth values used here, versus the partial
276 depth values reported previously, are attributable predominantly to the integration depth used.

277 We use the SOC stock data to estimate the amount of soil carbon removed by landslides. These data
278 may provide an upper estimate on the total amount of organic carbon derived from recently
279 photosynthesized biomass (i.e., “biospheric organic carbon”), partly because of the presence of
280 carbonate C and rock-derived organic carbon which is present in the catchment (Clark et al., 2013).
281 However, the contribution from these non-biospheric components is expected to be small given the
282 relatively low content of each compared to biospheric %OC, typically at concentrations of many
283 percent. Additional bias may arise from the location of plots within the catchment, specifically with
284 respect to topographic position (Marvin et al., 2014). The mean plot slopes range from 20° to 38°, as

285 measured from the 3 m x 3 m CAO DEM, so these sites capture a large slope range but are at the
286 lower slope end of the slopes found throughout the Kosñipata catchment (mean catchment slope of
287 38°). Data on soil OC stocks collected from a wide range in slopes at high elevations (near the tree
288 line) in the region of the Kosñipata Valley suggest there is not an evident slope-dependence that
289 would be likely to strongly bias our results (see Supplement Fig. S2) (Gibbon et al., 2010).

290

291 **3.3.3. Calculating fluxes of carbon stripped from hillslopes by landslides**

292 Carbon stocks for soil, above ground living biomass, and roots were calculated for elevation bands of
293 300 m, based on the relationships in Table 1. Landslide carbon flux (tC yr⁻¹) was determined by
294 multiplying the landslide rate in each elevation band (% yr⁻¹) by soil, AGLB, and root carbon stocks
295 (tC km⁻²) in the respective elevation band. We propagated the error on the elevation trends (from Fig.
296 7 and Table 1) to estimate uncertainty on the landslide-associated carbon flux by Gaussian error
297 propagation. The landslide C yield (tC km⁻² yr⁻¹) was calculated by summing all 300 m elevation
298 bands and normalising by the non-shadow catchment area (143 km²).

299 The calculations assume that landslides strip all above ground, root biomass and soil material from
300 hillslopes. This assumption is supported by field observations from the Kosñipata Valley that
301 landslides are cleared of visible vegetation and roots and are typically bedrock failures that remove
302 the entire mobile soil layer. To test this latter assumption, we used geometric scaling relationships for
303 landslides in mountainous terrain (Larsen et al., 2010) to estimate landslide depths. We calculated
304 landslide volume from the area (A)-volume (V) relationship, $V = \alpha A^\gamma$, where α and γ are scaling
305 parameters (we used $\alpha = 0.146$ and $\gamma = 1.332$, from the compilation of global landslides in Larsen et
306 al., 2010, but also tested other literature values). We estimated average depth by dividing volume for
307 each landslide by the respective landslide area.

308 **3.4. Landslide revegetation**

309 We classified landslides as being “revegetated” when they were dominated by a closed forest canopy
310 to an extent that we could no longer visually distinguish the landslide scar or bare ground in the 2 m
311 resolution WorldView-2 imagery (Blodgett and Isacks, 2007). We determined the fraction of area of
312 the landslides occurring in each year (beginning in 1988) that was no longer visible as of 2011, the
313 year with the latest high-resolution image (Fig. 8). Some landslides were revegetated as soon as four
314 years after occurrence. For landslide years prior to 2008, i.e. all landslide years with some observable
315 recovery, we ran a linear regression between landslide area revegetated (specifically, area of fully
316 revegetated landslides from a given year as a % of total landslide area from that year) and the number
317 of years that had passed since landslide occurrence (the difference between the given year and 2011).

318 This analysis used a total of 18 data points, one for each year between 1988 and 2007 except for 2
319 years that had no measured landslides (Fig. 8; Table S2).

320 The metric of visible revegetation that we use in this study provides a measurable index for assessing
321 ecosystem recovery from remote imagery. However, it does not necessarily mean complete
322 replenishment of above ground carbon stocks or regrowth of all vegetation to the extent present prior
323 to landslide removal. It is also likely to take longer than this time for replenishment of soil carbon
324 stocks to pre-landslide values (Restrepo et al., 2009).

325 **3.5. Topographic analysis**

326 We used two DEMs for topographic analysis. Slope angles and elevation statistics within the
327 Kosñipata catchment study area were calculated from the 3m x 3m CAO LiDAR-based DEM (see
328 Appendix A). For river channel analysis within the Kosñipata Valley and for all topographic analyses
329 in the wider Madre de Dios region, we used a 30 m resolution SRTM-derived DEM (Farr et al., 2007)
330 with holes patched using the ASTER GDEM (METI/NASA, 2009). We were not able to use the
331 higher-resolution CAO DEM for these calculations because it did not extend beyond the Kosñipata
332 catchment study area and contained gaps that made complete flow routing calculations problematic.

333 The dependence of calculated slope on grid resolution (Lin et al., 2008; Blodgett and Isacks, 2007;
334 Zhang and Montgomery, 1994) means that reported slope values inherently differ between the DEMs
335 used in this study, and when compared to values from the 90 m x 90 m SRTM-derived DEM (cf.
336 Clark et al. (2013)). In this study, we only compare results internally between values calculated from
337 the same DEM.

338

339 **4. Results**

340 **4.1. Landslide rates and role of a large rain storm in 2010**

341 Approximately 2% (2.8 km²) of the visible Kosñipata Valley study area experienced landslides over
342 the 25-year study period. This percentage of landslide area is similar to landslide coverage in the
343 Ecuadorian and Bolivian Andes (Blodgett and Isacks, 2007; Stoyan, 2000). Of the total landslide area
344 in the catchment, 97.1% was in the forested portion and the remaining 2.9% in the puna.

345 The mean valley-wide landslide rates were 0.076% yr⁻¹, when averaged across 1 x 1 km grid cells.
346 Rates ranged from no landslides detected to 0.85% yr⁻¹ for individual grid cells (Fig. 2b). The average
347 landslide rate corresponds to average hillslope turnover time of ~1320 yrs for the valley (Fig. 2c).
348 Values reported provide a minimum constraint on landslide rate and a maximum constraint on
349 turnover time, since small landslides and landslides under topographic shadow were excluded (see
350 Section 3.1). The landslide hillslope turnover time in the Kosñipata Valley is similar to the landslide

351 hillslope turnover time observed in the Waitangitona Basin of New Zealand, but is 2.3 times faster
352 than the mean landscape-scale landslide hillslope turnover in the western Southern Alps of New
353 Zealand (Hilton et al., 2011) and in Guatemala (Restrepo and Alvarez, 2006) and 24 times faster than
354 in Mexico and in Central America (Restrepo and Alvarez, 2006).

355 A single large-magnitude rainfall event on March 4th 2010 triggered 27% of all of the landslide area
356 observed during the 25-year study period in the Kosñipata study catchment. Rainfall during this storm
357 peaked at 94 mm hr⁻¹, with ~200 mm falling in 4 hr, recorded by a meteorology station at 1350 m
358 within the catchment (Fig. 9). The storm accounted for ~185 landslides with 0.75 km² cumulative
359 area. The annual total landslide area for 2010 was consequently much higher than for any other year
360 in the dataset (Fig. 3).

361 4.2. Spatial patterns of landslides

362 The histogram of catchment area in the Kosñipata catchment shows a skewed distribution with respect
363 to elevation, with greater area at lower elevations (Fig. 5a). The histogram of landslide area is shifted
364 to lower elevations compared to the catchment and shows a bi-modality. The 2010 landslides focused
365 almost exclusively at low elevations, below ~2600 m (Fig. 5c). Although the remaining landslides
366 over the 25-year study period located at low elevations relative to the catchment, they were at higher
367 elevations than the 2010 landslides. The bi-modality of the overall landslide distribution emerges
368 from the addition of the two nearly distinct distributions (Fig. 5c). Because of the small catchment
369 area at low elevations, overall landslide susceptibility is highest at the low elevations (particularly
370 <~1800 m) (Fig. 5b). When excluding the 2010 landslides, the high susceptibility at low elevations is
371 not evident, and the only clear trend is the very low landslide susceptibility at the highest elevations
372 (> 3500 m) (Fig. 5d). [Since our mapping did not distinguish landslide scars from deposits \(see](#)
373 [Section 3.1\), systematic changes in the ratio of scar to deposit area with elevation could influence](#)
374 [apparent patterns of landslide occurrence. For example, larger deposit areas at low elevation would](#)
375 [increase calculated susceptibility even if the total landslide scar area were not larger. However, our](#)
376 [anecdotal field observations do not suggest that landslides at lower elevations have consistently longer](#)
377 [run-out or larger deposit areas, so it is unlikely that such bias explains the observed relations between](#)
378 [landslide occurrence and topography within our inventory.](#)

379 The catchment area has a mean slope of 38° (calculated from the CAO DEM) and is skewed to lower
380 slopes (Figs. 2d, 6a). The distribution of landslide areas is shifted to slightly higher slopes compared
381 to catchment area and lacks the broad abundance at slopes <30°. The 2010 landslides show a similar
382 distribution with respect to slope as the landslides from all other years (Fig. 6c). In all cases, landslide
383 susceptibility increases sharply for slopes >30-40° (Fig.6d). All of the landslide data include areas at
384 low slopes, which we interpret as artefacts related to landslide deposits residing in valley bottoms,
385 since our mapping routines [did](#) not distinguish scars from deposits.

386 | **4.3. Catchment topographic characteristics**

387 | The Kosñipata catchment is characterized by a prominent vertical step knickpoint between
388 | approximately 1600 and 1400 m elevation (Fig. 10a). This knickpoint marks an inflection in the
389 | relationship between upstream drainage area and the slope of the river channel, characteristic of the
390 | transition from colluvial to bedrock or alluvial channels in mountainous settings (Whipple, 2004;
391 | Montgomery and Buffington, 1997) although we recognize that processes such as debris-flow incision
392 | may also influence the form of these relations (Stock and Dietrich, 2003). We used flow routing to
393 | separate the catchment into those slopes that drain into the river system upstream of this transition
394 | zone (as defined by the elevation at the top of the vertical step knickpoint) and those slopes that drain
395 | into the river system downstream of the transition (Fig. 10b). Hillslope angles are, on average, steeper
396 | downstream of the transition than upstream, and the distribution of slope angles downstream lacks the
397 | prominent bulge at relatively low slopes that is observed upstream of the transition. The general
398 | features observed in the Kosñipata study catchment, specifically the transition in the slope-area curves
399 | and the related shift in hillslope angles, also generally characterize the other major rivers draining
400 | from the eastern flank of the Andes in the Alto Madre de Dios (Fig. 11).

401 | **4.4. Catchment-scale carbon stocks and stripping of carbon by landslides**

402 | The estimated catchment-scale carbon stock for the Kosñipata Valley is $\sim 34\,670 \pm 4545$ tC km⁻², with
403 | $\sim 27\,680 \pm 4420$ tC km⁻² in soil and $\sim 5370 \pm 840$ tC km⁻² in vegetation (Fig. 7). We estimate that
404 | epiphyte (Horwath, 2011) and woody debris (Gurdak et al., 2014) biomass adds an additional ~7% of
405 | carbon (<5% from epiphytes and <3% from woody debris; Fig. 7c). Overall, the vegetation carbon
406 | stock values from the Kosñipata Valley are slightly lower than lowland tropical forests, and the soil
407 | values higher (Dixon et al., 1994), which is consistent with broad trends in the tropics in which soil
408 | carbon stocks increase with elevation and are frequently greater than vegetation carbon stocks
409 | (Gibbon et al., 2010; Raich et al., 2006).

410 | Averaged over the 25-year duration across the 143 km² non-shadowed catchment area, the estimated
411 | total flux of carbon stripped from hillslopes by landslides was 3700 ± 510 tC yr⁻¹, with 2880 ± 500 tC yr⁻¹
412 | ¹ derived from soil and 820 ± 110 tC yr⁻¹ from vegetation (Fig. 12a). In terms of area-normalized yield
413 | of carbon, landslides stripped 26 ± 4 tC km⁻² yr⁻¹ from hillslopes, with 20 ± 3 tC km⁻² yr⁻¹ derived from
414 | soil and 5.7 ± 0.8 tC km⁻² yr⁻¹ from vegetation (Table 2; Fig. 12b). These values may underestimate
415 | total catchment-wide fluxes because our landslide mapping process missed a proportion of small,
416 | numerous landslides (see Fig. 4, Section 3.1).

417 | On the other hand, our values may overestimate fluxes from soil OC if landslides are shallower than
418 | soil depths, since we have assumed complete stripping of soil material to full soil depth and since soil
419 | OC stocks depend on depth of integration (see Section 3.3, above). The deepest average soil depths
420 | observed in the plots used in this study were 1.58 m (Table S3). Using average scaling parameters for

421 global landslides (Larsen et al., 2010), only 99 landslides in our inventory, equating to 0.06 km² total
422 landslide area (or ~2% of total landslide area), would be shallower than these deepest soils at 1.58 m.
423 Using scaling parameters for bedrock landslides only ($\alpha = 0.146$ and $\gamma = 1.332$; Larsen et al. (2010),
424 results in only one landslide shallower than 1.58 m. This analysis corroborates our field observations
425 that most landslides in the Kosñipata Valley clear soil from hillslopes and expose bedrock. We thus
426 view our calculation of fluxes on the basis of complete stripping of soil as providing a reasonable
427 estimate.

428 Our calculation of landslide-associated carbon fluxes includes carbon that was previously residing
429 both on landslide scars and in areas of landslide deposits. The fate of carbon from each of these areas
430 may differ, but such differences are not well known and we consider all to contribute to the loss of
431 previously living biomass as a result of landslide occurrence. When considering carbon budgets at the
432 landscape-scale, the landslide-associated carbon fluxes we report here should also be viewed in the
433 context that other processes such as soil creep may additionally contribute to the transfer of carbon
434 from hillslopes to rivers (e.g., (Yoo et al., 2005).

435

436 **5. Discussion**

437 **5.1. The geomorphic ‘work’ of storm-triggered landslides in the Kosñipata Valley**

438 The March 2010 storm clearly stands out as the most significant landslide event that occurred during
439 the duration of this study. We lack a precipitation record for the full 25-year study period, but it is
440 probable that this storm was the largest single precipitation event during that time. Landslides
441 triggered in 2010 account for 0.75 km², or 27% of the total landslide area during the 25-year study
442 period, and these landslides stripped 25,500 tC from hillslopes, equivalent to 26% of the total. The
443 quantitative importance of this individual storm in our dataset is consistent with observations of
444 storm-triggering of intense landslides elsewhere (Wohl and Ogden, 2013; Ramos Scharrón et al.,
445 2012; West et al., 2011; Casagli et al., 2006).

446 The annual resolution of our observations of landslide rates in the Kosñipata Valley makes it possible
447 to consider how the geomorphic work done in this relatively infrequent but high magnitude event
448 compares to the work done in smaller but more frequent events. Here we define geomorphic work,
449 *sensu* Wolman and Miller (1960), as total landslide area, reflecting the removal of material from
450 hillslopes (rather than, for example, the work done by landslides to modify slope angles). Across the
451 25-year dataset, we estimate the return time or recurrence interval RI (i.e., how frequently a year of
452 given total landslide magnitude would be expected to occur), as $RI_i = (n+1)/m_i$, where RI_i is the return
453 interval for the year with the i^{th} largest total annual landslide area, n is the total length of the record
454 (25 years in this study) and m_i is the rank order of year i within the dataset in terms of total landslide

455 area. Thus 2010, the year with most landslide area, has $RI = 26$ years, while years characterized by
456 lower landslide area have more frequent inferred recurrence intervals. When the annual data for
457 landslide area are plotted as a function of RI (Fig. 3b), 2010 is clearly at the highest magnitude, as a
458 result of the March 2010 storm. Even so, the landslide area from 2010 still falls on an approximately
459 linear (power law exponent ~ 1) trend coherent with the rest of the dataset. We do not have high
460 enough temporal resolution to analyse the effects of individual storms in detail, as would be preferred
461 for a robust recurrence interval analysis. Nonetheless, the linearity of the relationship for annual
462 landslide areas suggests that even as the frequency of large storm events in the Kosñipata Valley
463 decreases, the landslide area associated with these events may increase commensurately, such that the
464 effects compensate.

465 We can further explore the amount of work done, again in terms of landslide area, by the cumulative
466 effect of repeated events of small magnitude versus occasional events of larger magnitude. We
467 calculate the % work done for a year with a given recurrence interval as $W_i = (A_i/\Sigma A)/RI_i \times 100$,
468 where A_i is the landslide area in year i and ΣA is the total landslide area in the full dataset. When W_i is
469 plotted versus RI_i , the compensating effect of frequency and magnitude is evident (Fig. 3c). With the
470 exception of the most frequent years that are characterized by very little landslide activity (low RI and
471 low W), most years are characterized by a fairly similar value of W . Thus we expect that the long-
472 term total landslide area resulting from years characterized by storm activity of varying magnitude is,
473 on average, very similar in this setting. In other words, the landslide work done in years with rare,
474 large storms is more or less similar to the sum of the total integrated work done in those years with
475 smaller but more frequent storms.

476 Many previous studies of storm-triggered landslides have focused specifically on storm events (e.g.,
477 (Wohl and Ogden, 2013; Ramos Scharrón et al., 2012; West et al., 2011) and lacked such longer-term
478 context, although several studies on storm triggers of landslides have been concerned with identifying
479 threshold storm intensities for failure (e.g., (Guzzetti et al., 2007; Glade, 1998; Larsen and Simon,
480 1993). Time series with higher temporal resolution associated with individual storm events of varying
481 magnitude rather than annual total landslide areas as used in this study would provide a test of the
482 inferences made here, and analyses similar to that in this study for storm-triggered landslides in other
483 settings would help shed more light on how storms contribute to erosional processes in mountain
484 landscapes. Nonetheless, even though the total work done by large magnitude storms may not exceed
485 that done by smaller events over the long term, the immediacy of large storm effects may be
486 important from the perspectives of hazards, fluvial impacts, and biogeochemical processes. For
487 example, large events will supply large amounts of clastic sediment (Wang et al., 2015) and organic
488 material (West et al., 2011) in a short space of time.

489 **5.2. Spatial patterns of landslide activity**

490 **5.2.1 Spatial patterns and their relation to the 2010 storm**

491 Spatial and temporal patterns of landslides depend on proximal triggers such as rainfall and seismic
492 activity (Lin et al., 2008; Meunier et al., 2008; Densmore and Hovius, 2000), as well as on
493 geomorphic pre-conditions, such as bedrock strength and slope angle, the latter of which is at least in
494 part regulated by fluvial incision by rivers (Larsen and Montgomery, 2012; Bussmann et al., 2008;
495 Lin et al., 2008). The observation of highest landslide susceptibility in the Kosñipata Valley at highest
496 slopes in the catchment reflects the importance of slope angle for landslide failure. The notable shift
497 from low to high landslide susceptibility above 30-40° (Fig. 6b) is consistent with the hillslope angles
498 that reflect rock strength expected for the metamorphic and plutonic bedrock (Larsen and
499 Montgomery, 2012). Generally, the greater overall landslide susceptibility at the lower elevations in
500 the Kosñipata Valley is consistent with the higher slope angles at these elevations (Figs. 2, 5, 10b).
501 This set of observations is consistent with predictions of a threshold hillslope model (cf. Gallen et al.
502 (2015); Roering et al. (2015); Larsen and Montgomery (2012)).

503 In more detail, the distribution of landslides with respect to elevation in the Kosñipata Valley is
504 complicated by clustering of the 2010 storm-triggered landslides at low elevations. This clustering
505 may be explained at least in part by the focused intensity of the 2010 storm precipitation at low
506 elevations; much lower rainfall was recorded on March 4th at a meteorology station at 2900 m
507 elevation in the Kosñipata Valley (at the Wayqecha forest plot), compared to the San Pedro
508 meteorological station at 1450 m elevation (Fig. 9a). Although the single 2010 event may not
509 contribute more to the development of long-term landslide area than the cumulative effect of smaller
510 events (see above), the landslides from this one specific event do significantly influence the overall
511 spatial distribution of landslides visible in present-day imagery. One implication of this observation is
512 that landslide maps based on all visible landslides at any one point in time, assuming uniform rates of
513 occurrence, may overlook the role of specific proximal triggering events that lead to spatial clustering.
514 Such event-clustering may influence inferred relationships between landslides and controlling factors
515 such as regional precipitation gradients or patterns of uplift, emphasizing that time-sequence of
516 landslide occurrence may be important to accurately assessing such relationships.

517 **5.2.2 Storm triggered landslides at low elevations: Stochastic happenstance or characteristic of** 518 **long-term erosional patterns?**

519 The elevation distribution of landslides in the 2010 storm is clearly distinct from the background
520 landslide activity during the 25-year study period. This difference raises an important question: are the
521 2010 landslides representative of a distinct spatial pattern associated with larger storm events? Or are
522 the spatial locations of these landslides reflective of one stochastic storm event that happened to be
523 captured in our analysis and is part of a series of events that shift in location throughout the catchment
524 over time? We cannot distinguish these possibilities conclusively, but we do have some evidence that

525 allows for preliminary inferences that could be tested with further work. Two lines of evidence
526 suggest that the focusing of storm-triggered landslides at low elevations in the Kosñipata study
527 catchment may be characteristic of long-term spatial patterns in which routine landslides occur
528 throughout the catchment while rarer, intense landslide events selectively affect the lower elevations.

529 The first line of evidence is that the magnitude-frequency statistics for precipitation indicate that low-
530 frequency events of high-magnitude (i.e., relatively infrequent but large storms) are more
531 characteristic at low elevation sites compared to high elevations (Fig. 9b). This statistical tendency
532 toward more storm activity at low elevations would provide a mechanism for regular storm-triggering
533 of landslides at these elevations.

534 A second set of information comes from the Kosñipata Valley topography and its relation to implied
535 erosion associated with landslide activity. Although total landslide area in our Kosñipata dataset is
536 greatest at mid-elevations, these mid-elevation landslides are distributed over a relatively large
537 catchment area (Fig. 5a). Effective landslide erosion is greatest where landslide susceptibility on a
538 unit-area basis is highest (Fig. 5b), so our inventory implies focused landslide erosion at lower
539 elevations (<~1500-2000 m) in the Kosñipata Valley, specifically associated with the 2010 storm
540 (Figs. 2a, 5). This focused erosion appears to spatially coincide with the observed transition in the
541 river channel profile at ~1700 m elevation, marked by the vertical step knickpoint (Fig. 10a). In the
542 Kosñipata Valley, this transition occurs near a lithological change from sedimentary to plutonic
543 bedrock. However, as best known the lithological contact does not exactly coincide spatially with the
544 knickpoint, and the other principal rivers in the region are also characterised by similar transitions in
545 channel morphology even though they do not have the same lithological transition, suggesting that
546 lithology is not the primary control on the observed transition in channel morphology (Fig. 11).

547 Several other processes can generate knickpoints in river profiles (e.g., (Whipple, 2001). The
548 topographic transition in the Kosñipata and in neighbouring catchments appears to approximately
549 coincide with changes in precipitation regime, and specifically with less cloud cover and greater storm
550 occurrence below the level of most persistent annual cloud cover in the Andean mid-elevations. (cf.
551 Espinoza et al. (2015); Rohrmann et al. (2014) for the southern central Andes). By increasing
552 erosional efficiency, this climatic transition may at least in part contribute to generating the observed
553 channel profile. Other effects may also be important, for example the transient upstream propagation
554 of erosion driven by past changes in uplift, as proposed for the eastern Andes in Bolivia (Whipple and
555 Gasparini, 2014), or unidentified geologic structures in the Alto Madre de Dios region. These
556 possibilities are discussed further below.

557 Whatever the underlying cause, hillslope angles downstream of the transitions in channel morphology
558 are generally steeper than those upstream (Figs. 10b and 11c), consistent with the downstream slopes
559 being more prone to landslide failure over the long term. The total area of landslides triggered on low-

560 elevation slopes in 2010 does not exceed the accumulated landslide area in the rest of the catchment
561 over the longer term (see discussion of magnitude-frequency above, and histograms of landslide area
562 in Fig. 5a). Nonetheless, these low-elevation landslides are concentrated in a smaller area (Fig. 5b)
563 and therefore represent higher landslide susceptibility, greater rates of landscape lowering and more
564 frequent hillslope turnover.

565 Based on the consistency of catchment topography with the landslide distribution that includes 2010
566 storm-triggered landslides, we speculate that the high rates of landslide erosion at low elevations in
567 the Kosñipata catchment are characteristic of long-term erosional patterns. This hypothesis could be
568 tested by complementing the landslide analysis presented in this study with measurements of long-
569 term denudation rates in small tributary basins of the Kosñipata Valley above and below the apparent
570 morphologic transition. Although we acknowledge that we currently lack such supporting
571 independent evidence, in the following sections we include consideration of some of the possible
572 implications of our hypothesized ~~erosional~~ transition towards higher landslide occurrence ~~and~~
573 ~~associated erosion~~ at lower elevations in the Kosñipata Valley.

574 **5.3. Landslide-driven erosion and regional topography**

575 In general terms, high-elevation, low-slope surfaces, such as those that characterize the upper portions
576 of the Kosñipata Valley, are thought to have a number of possible origins, including (i) the uplift and
577 preservation of previously low-lying “relict” surfaces (e.g., (Clark et al., 2006), (ii) glacial “buzz-saw”
578 levelling of surfaces near the glacial equilibrium line altitude (Brozović et al., 1997), (iii) erosion of
579 rocks with contrasting strength (e.g., (Oskin and Burbank, 2005), and (iv) in situ generation through
580 river system reorganization over time (Yang et al., 2015). There is no evidence for a glacial or
581 lithological cause for low-relief parts of the Kosñipata Valley and the immediately adjacent portions
582 of the Andean plateau, suggesting either a relict origin or in situ fluvial formation. Similar high-
583 elevation, low-relief surfaces south of our study region, along the eastern flank of the Andes in
584 Bolivia, have been proposed as relict landscapes uplifted in the past ~10-12 Myrs (Whipple and
585 Gasparini, 2014; Barke and Lamb, 2006; Gubbels et al., 1993). By this interpretation, erosion into the
586 eastern Andean margins has generated escarpments but not yet erased the original surfaces (Whipple
587 and Gasparini, 2014).

588 From landslide mapping in the Kosñipata Valley, we infer higher hillslope erosion rates at lower
589 elevations and particularly downstream of the knickpoint in this catchment. Even when ignoring the
590 very low-elevation landslides associated with the 2010 storm in our dataset, the occurrence of
591 landslides throughout the 25-year study period are notably shifted to lower elevations compared to the
592 Kosñipata catchment area (Fig. 5c). This pattern emphasizes that erosion rates are low at the highest
593 elevations, where slopes are also lower presumably because incision is less pronounced. If our
594 observed landslide rates reflect long-term erosion, these observations are consistent with the idea that

595 the low slopes at high elevations in this region of the Andes are preserved because propagation of
596 more rapid erosion at low elevations has not yet reached the low-slope parts of the landscape. But,
597 based on the distribution of landslide erosion alone, we cannot distinguish whether the low slope
598 regions have their origin as relict landscapes or features resulting from fluvial reorganization.

599 The importance of storm triggering for setting the spatial patterns of landslide activity in the
600 Kosñipata Valley suggests that greater storm frequency (e.g., Fig. 9b) could be an important
601 mechanism facilitating higher erosion rates at low elevations in this catchment, consistent with
602 climate variability being a major erosional driver (DiBiase and Whipple, 2011; Lague et al., 2005).
603 The indication of a mechanistic link between precipitation patterns and erosion in the Kosñipata
604 catchment may provide clues about how climatic gradients leave an imprint on the topography of the
605 eastern Andes (e.g., (Strecker et al., 2007), potentially superimposed on tectonically-controlled
606 patterns of transient erosion into the uplifted mountain range (Gasparini and Whipple, 2014).
607 Although previous studies have considered the role of gradients in precipitation magnitude across
608 strike of the eastern Andes (e.g, Gasparini and Whipple (2014); Lowman and Barros (2014)), we note
609 that little work has considered the role of storm frequency, which our analysis suggests may be
610 variable and important in setting erosion patterns in this region.

611 Based on our landslide dataset and the precipitation statistics for the Kosñipata Valley, we speculate
612 that the greater precipitation magnitude and frequency of large storm events below the cloud
613 immersion zone in the eastern Andes of the Madre de Dios basin work to facilitate a combination of
614 hillslope failure, sediment removal, and river channel incision. Channel incision, facilitated by high
615 storm runoff and the tools provided by landslide erosion (e.g., (Crosby et al., 2007), increases
616 hillslope angles, and landslide failure keeps pace, triggered by storm events such as the 2010 event
617 observed in our dataset. Focused, climatically controlled erosion at lower elevations along the eastern
618 flank of the Andes in the Madre de Dios basin could contribute to the preservation of relatively low-
619 slope surfaces at high elevations: if rates of erosion in and above the cloud immersion zone are limited
620 by decreased precipitation and particularly reduced storm frequency, the upstream propagation of
621 erosion may be inhibited, reducing the potential for rivers to incise into the low slope regions in the
622 high-elevation headwaters. This, in turn, may explain why rivers along the eastern flank of the Andes
623 in Peru have not succeeded in eroding back into the Andean topography sufficiently to “capture” the
624 flow of the Altiplano rivers (e.g., the tributaries of the Rio Urubamba that currently flow several
625 hundred kilometres to the north via the Ucayali before cutting east through the Andes to join the
626 Amazonas). Our results thus raise the possibility of a potential climatic mechanism for sustaining this
627 topographic contrast and prolonging the persistence of the asymmetric morphology in this region of
628 the Andes.

629 **5.4. Landslide transfer of organic carbon to rivers**

630 The 26±4 tC km⁻² yr⁻¹ of organic carbon stripped from hillslope soil and vegetation during our study
631 period reflects a significant catchment-scale carbon transfer (Stallard, 1998). The area-normalized
632 landslide carbon yield in the Kosñipata Valley is similar to the upper end of values for other mountain
633 sites around the world where analogous carbon fluxes have been evaluated. For example, in a region
634 of Guatemala with a 20-year hurricane return time, landslide carbon yields were 33 tC km⁻² yr⁻¹
635 (Ramos Scharrón et al., 2012), similar to our Kosñipata results. In the western Southern Alps of New
636 Zealand, landslide carbon yields were 17 ± 6 tC km⁻² yr⁻¹ in catchments where landslide rates were
637 highest, while the mean yield was much lower, at ~8 tC km⁻² yr⁻¹ (Hilton et al., 2011). In part, the high
638 carbon flux we observe in the Kosñipata Valley reflects the high organic carbon stocks of soils in this
639 catchment (27 680 ± 4 420 tC km⁻²), larger than the mean estimated in the western Southern Alps,
640 New Zealand (18 000 ± 9 000 tC km⁻²) (Hilton et al., 2011). The high flux can also be attributed to the
641 high rates of landsliding driven by the combination of steep topography and intense precipitation
642 events (and presumably on multi-centennial timescales by large earthquakes).

643 Following the recolonization of landslide scars (Fig. 8), the fate of landslide-derived organic carbon
644 governs whether erosion acts as a source or sink of carbon dioxide to the atmosphere (Ramos
645 Scharrón et al., 2012; Hilton et al., 2011). Bedrock landslides may supply organic carbon to rivers at
646 the same point in time and space as large amounts of clastic sediment are delivered from hillslopes
647 (Hilton et al., 2011; Hovius et al., 1997). The association of organic matter with high mineral loads
648 enhances its potential for sedimentary burial and longer-term sequestration of atmospheric carbon
649 dioxide (Galy et al., 2015; Hilton et al., 2011). In contrast, oxidation of biospheric organic carbon
650 eroded by landslides represents a poorly quantified source of CO₂ for assessments of ecosystem
651 carbon balance.

652 The extent to which landslides connect to river channels exerts a first-order control on the fate of
653 landslide material (Dadson et al., 2004), and thus on the fate of carbon. We identified landslides as
654 connected or unconnected to rivers by manually inspecting high-resolution imagery and following
655 landslides to their termination (i.e. to their lowest elevation point). Connected landslides terminated in
656 river channels, identifiable by the absence of vegetation. We found that, for the Kosñipata Valley
657 during our study period, greater than 90% of landslides were directly connected with rivers, similar to
658 the high connectivity found for other storm-triggered landslides (e.g., (West et al., 2011). However,
659 even with high connectivity, it remains uncertain in the case of the Kosñipata how much of the
660 material stripped by landslides is actually removed by rivers and exported out of the valley.

661 While quantifying the onward fluvial transfer of organic carbon stripped by landslides and its fate in
662 the Madre de Dios River and wider Amazon Basin is out of the scope of the present study, our
663 observations provide baseline data for interpreting river flux measurements, as well as important new
664 insight on the role of landslides in the routing of organic carbon in mountain catchments. First, we

665 note that the location of landslides within a catchment may influence whether the organic material
666 eroded from hillslopes is transported by rivers (Hilton et al., 2008b). The observation that landslide
667 erosion may be non-uniform thus has important implications for organic carbon fate. In lower-order
668 streams, landslides may be less likely to connect to rivers (Ramos Scharrón et al., 2012), and rivers
669 are less likely to have capacity to export material, compared to higher order streams. In the Kosñipata
670 River, focused erosion of organic carbon occurs in the low/mid-elevations and is likely to act to
671 enhance delivery into higher order river channels, optimizing the potential for removal from the river
672 catchment. For instance, the mid-elevations (2100 m to 3000 m) are the source of the majority (51%)
673 of the organic material (in terms of mass per time) eroded from hillslopes by landslides, because these
674 elevations cover the greatest proportion of total basin area (43%) (Fig. 12a). On a per-area basis (i.e.,
675 in $\text{tC km}^{-2} \text{ yr}^{-1}$), landslide mobilisation of organic carbon is most frequent at lower elevations (Fig.
676 12b); while the land area in the Kosñipata study area below 1800 m elevation comprises 9% of the
677 total catchment area, 18% of the organic material stripped by landslides comes from these elevations
678 (Figs. 12a, 12b).

679 | Second, the landslide-derived organic carbon yield is mostly (80%) derived from soil organic matter.
680 This material is finer-grained than coarse woody debris and is thus more likely to be entrained and
681 transported by the Kosñipata River. This observation is consistent with measurements of the isotopic
682 and elemental composition of river-borne particulate organic carbon (POC) in this catchment, which
683 suggest that soil organic carbon from upper horizons appears to be a significant source of biospheric
684 POC (Clark et al., 2013). While the total POC export fluxes from the Kosñipata River are still to be
685 quantified, it is likely that the landslide process offers a mechanism by which large quantities of
686 organic matter, and particularly fine-grained soil organic matter susceptible to fluvial transport, can be
687 supplied from steep hillslopes to river channels.

688 Finally, our observations are important for understanding the episodic delivery of Andean-derived
689 organic matter to river systems via the landslide process. The distinct focusing of 2010 rain storm-
690 driven erosion at low elevations of the Kosñipata study catchment demonstrates the potential for
691 landslides triggered by individual storm events to erode material selectively from within a
692 catchment's elevation range. Measurements of biomarker isotope composition in downstream river
693 sediment have shown that organic erosional products reflect distinct elevation sources during storms
694 (Ponton et al., 2014). Together, these results emphasize the potential role for storm events to
695 determine the organic biomarker composition delivered to sediments and to introduce biases relative
696 to the uniform catchment integration often assumed of erosion (Bouchez et al., 2014; Ponton et al.,
697 2014).

698 **5.5. Timescales of re-vegetation and implications for ecosystem disturbance and composition**

699 The biomass and soil removed by landslides is regenerated on hillslopes over time. The duration and
700 dynamics of vegetation recovery influence vegetation structure and soil structure, provide habitat for
701 various species, play an integral role in nutrient cycling, and determine the timescale over which
702 standing stocks of organic carbon are replenished (Restrepo et al., 2009; Bussmann et al., 2008). For
703 the Kosñipata study catchment, we estimate that 100% of the landslide area from a given year reaches
704 full vegetation cover that is indistinguishable from the surrounding vegetation (based on observable
705 changes from 1988 to 2011 in remote sensing imagery) at $\sim 27 \pm 8$ yrs after landslide occurrence (Fig.
706 8). Individual landslides showed large variability; one landslide with a very large area at high
707 elevation, visible in an air photo from 1963, is still visible with active portions in 2011, indicating that
708 at least portions of very large landslides may take longer (>48 yrs) to revegetate, partly due to
709 reactivation. On the other hand, the shortest revegetation time for a landslide occurred within 4 years.
710 In the Bolivian Andes, at sites with similar montane forest and similar elevation range, similar
711 revegetation times of 10 to 35 yrs were estimated based on dating trees on landslide scars and
712 evaluating canopy closure in aerial photographs (Blodgett and Isacks, 2007).

713 Although the return to vegetation cover on landslide scars may occur over several decades, it may
714 take much longer, perhaps hundreds of years, to reach the full maturity of a tropical montane cloud
715 forest and to fully replenish soil carbon stocks (Walker et al., 1996). Post-landslide vegetation
716 modelling in the Ecuadorian Andes (1900-2100 m) suggested that initial return of vegetation to
717 landslide surfaces occurs within 80 years after a landslide but that it takes at least 200 years for the
718 post-landslide forest to develop the biomass of a mature tropical montane forest (Dislich and Huth,
719 2012). The timescale of this full maturation process may be important when considering the impact of
720 landslides on carbon budgets and ecosystem dynamics.

721 Repeated cycles of landslide activity and re-vegetation have the potential to introduce disturbance to
722 ecosystems that may affect soil nutrient status, carbon stocks, and even plant biodiversity (Restrepo et
723 al., 2009). Patches of bare rock left by landslides undergo ‘quasi-primary’ succession (Restrepo et al.,
724 2009) that promotes movement of organisms and ecosystem reorganisation (Walker et al., 2013;
725 Hupp, 1983), while inhibiting ecosystem retrogression and nutrient depletion (Peltzer et al., 2010). On
726 landslides in the Bolivian Andes, plant species richness increased from early to late succession and
727 then declined in very mature or senescent forests (Kessler, 1999).

728 In the Kosñipata Valley, the spatial trends in landslide rate with elevation are similar to trends in plant
729 species richness measured at forest plots (Fig. 13). Similar to landslide activity, species richness is
730 lowest at high elevations, increases slightly with decreasing elevation to 2000 m, and then increases
731 abruptly (from 80 to 180 species ha^{-1}) on forested hillslopes between 2000 m and ~ 1700 m (Fig. 13).
732 The coincidence of these patterns may reflect the control of both landslides and biodiversity by
733 climatic conditions (e.g., both greater landslide activity and greater biodiversity below the cloud

734 immersion zone). Or the patterns may be simply coincidental, with biodiversity regulated by factors
735 independent of landslide erosion, such as light and temperature, or the transition between
736 lowland/submontane species and montane cloud forest species. We suggest that it may also be
737 possible that the intermediate disturbance regime (Connell, 1978) associated with landslide activity at
738 the lower catchment elevations influences ecosystem structure (Walker et al., 2013; Restrepo et al.,
739 2009; Kessler, 1999; Hupp, 1983) and contributes to enhanced biodiversity observed below ~1700 m.
740 Such effects could be consistent with peaks in species richness at mid-elevations (around 1500 m)
741 observed across Andean forest plots in Peru (Fig. 13), Bolivia, and Ecuador (Engemann et al., 2015;
742 Salazar et al., 2015; Girardin et al., 2014b; Huaraca Huasco et al., 2014). A complex mix of
743 geomorphic, climatic and ecological factors likely influence landslide and biodiversity patterns, but
744 coincidence in our dataset provides impetus for future studies of species diversity along
745 geomorphically-imposed gradients of disturbance.

746

747 7. Conclusions

748 We have quantified the spatial and temporal patterns of landslides over 25-years in the Kosñipata
749 Valley, a forested mountain catchment in the Peruvian Andes. Over the 25 year period, one extreme
750 rainfall event in 2010 triggered ~1/4 of all inventoried landslides, demonstrating the importance of
751 large rainfall events for landslide activity in the Andes. The annual data from this study suggest that
752 the cumulative landslide area associated with smaller, more frequent storms may be similar to the area
753 associated with larger, rarer storms.

754 The landslides mobilized significant amounts of carbon from forested hillslopes, with an average
755 yield of 26 ± 4 tC km⁻² yr⁻¹. This is one of the largest erosive fluxes of biospheric carbon recorded in a
756 mountain catchment. We estimate that a large proportion of this material was from soil organic matter
757 (20 ± 3 tC km⁻² yr⁻¹) scoured from depths of ~1.5m or less, with above- and below-ground biomass
758 marking a smaller, yet still important contribution (5.7 ± 0.8 tC km⁻² yr⁻¹). That coupled with the
759 observation that ~90% of the mapped landslide areas were spatially connected to river channels
760 suggests that this biospheric carbon may be very mobile, and may contribute importantly to suspended
761 sediment export by the Kosñipata River. The onward fate of this carbon will play an important role in
762 determining whether landsliding and physical erosion processes in the Andes contributes a net carbon
763 dioxide source or sink.

764 Landslides observed in this study were not distributed uniformly across the catchment area, but were
765 focused on slopes above a threshold angle (ca. 30-40°), consistent with previous studies and
766 theoretical expectations. The highest elevations in the catchment are characterized by low slopes and
767 relatively little landslide activity. Landslides triggered by the large storm in 2010 cluster at low
768 elevations, where precipitation magnitude-frequency relations and catchment morphology hint that

769 such pulses of intense erosional activity may be characteristic of long-term patterns. Such non-
770 uniform erosion would have implications for sources and composition of sediment, organic matter and
771 associated biomarkers and could potentially contribute to influencing forest species composition
772 through patterns of disturbance. Relations between storm activity, landsliding and landscape processes
773 and ecological function merit further investigation to probe these possible links.
774

775 **Appendix A. High-resolution Digital Elevation Model**

776 For analysing the topography of the Kosñipata study catchment, we used a DEM generated from the
777 Carnegie Airborne Observatory 2 (CAO-2) next generation Airborne Taxonomic Mapping System
778 (AToMS) with an Airborne Light Detection and Ranging (LiDAR) (Asner et al., 2012). The CAO
779 data was processed to 1.12 m spot spacing. Laser ranges from the LiDAR were combined with the
780 embedded high resolution Global Positioning System-Inertial Measurement Unit (GPS-IMU) data to
781 determine the 3-D locations of laser returns, producing a ‘cloud’ of LiDAR data. The LiDAR data
782 cloud consists of a very large number of georeferenced point elevation estimates (cm), where
783 elevation is relative to a reference ellipsoid (WGS 1984). To estimate canopy height above ground,
784 LiDAR data points were processed to identify which laser pulses penetrated the canopy volume and
785 reached the ground surface. We used these points to interpolate a raster digital terrain model (DTM)
786 for the ground surface. This was achieved using a 10 m x 10 m kernel passed over each flight block;
787 the lowest elevation estimate in each kernel was assumed to be ground. Subsequent points were
788 evaluated by fitting a horizontal plane to each of the ground seed points. If the closest unclassified
789 point was $< 5.5^\circ$ and < 1.5 m higher in elevation, it was classified as ground. This process was
790 repeated until all points within the block were evaluated. The cell resolution was derived from the
791 DEM resampled in ArcGIS to a 3 m x 3 m DEM to smooth the topography from a 1.12 m x 1.12 m
792 DEM. Cells in the topographic shadow area and the area of the catchment with a gap in the data (~ 3
793 km^2 centralised in the upper elevations) were removed from this analysis.

794

795 *Author contributions.* K. E. Clark, A. J. West, R. G. Hilton, Y. Malhi, M. New, M. R. Silman, and S.
796 S. Saatchi designed the study; G. P. Asner and R. E. Martin carried out Carnegie Airborne
797 Observatory (CAO) data acquisition and analysis; C. A. Quesada carried out the soil stock fieldwork
798 and geochemical analysis; W. Farfan-Rios and M. R. Silman carried out the above ground living
799 biomass and plant species diversity fieldwork; A. B. Horwath carried out the bryophyte carbon stock
800 fieldwork; K. Halladay carried out the MODIS cloud cover analysis; K. E. Clark carried the analysis
801 under the advisement of A. J. West and with contributions from Y. Malhi and R. G. Hilton. K. E.
802 Clark and A. J. West prepared the manuscript with contributions from all of the co-authors.

803

804

805 **Acknowledgements**

806 This paper is a product of the Andes Biodiversity and Ecosystems Research Group (ABERG). KEC
807 was funded by the Natural Sciences and Engineering Research Council of Canada (NSERC) and
808 Clarendon Fund PhD scholarships. AJW was supported to work in the Kosñipata Valley by NSF-EAR
809 1227192 and RGH was supported by a NERC New Investigator Grant (NE/I001719/1). YM is
810 supported by the Jackson Foundation and a European Research Council Advanced Investigator Grant
811 GEM-TRAIT. The Carnegie Airborne Observatory is made possible by the Avatar Alliance
812 Foundation, Grantham Foundation for the Protection of the Environment, John D. and Catherine T.
813 MacArthur Foundation, Gordon and Betty Moore Foundation, W. M. Keck Foundation, Margaret A.
814 Cargill Foundation, Mary Anne Nyburg Baker and G. Leonard Baker Jr., and William R. Hearst III.
815 We thank D. Knapp, T. Kennedy-Bowdoin, C. Anderson, and R. Tupayachi for CAO data collection
816 and analysis; M. Palace for the QuickBird-2 satellite images from 2009 and 2010; S. Abele for GIS
817 advice; S. Moon and G. Hilley for providing Matlab code for slope-area analysis; and S. Feakins and
818 reviewers of a prior submission for comments. We thank Ken Ferrier and an anonymous referee for
819 their helpful and insightful reviews.

820

821

822 **References**

- 823 ACCA: Weather data San Pedro station, Asociación para la conservación de la cuenca Amazónica
 824 <http://atrium.andesamazon.org/index.php>, (accessed 01/04/2012), 2012.
- 825 Asner, G. P., Powell, G. V., Mascaro, J., Knapp, D. E., Clark, J. K., Jacobson, J., Kennedy-Bowdoin, T.,
 826 Balaji, A., Paez-Acosta, G., and Victoria, E.: High-resolution forest carbon stocks and
 827 emissions in the Amazon, *P Natl. Acad. Sci. USA*, 107, 16738-16742,
 828 10.1073/pnas.1004875107, 2010.
- 829 Asner, G. P., Knapp, D. E., Boardman, J., Green, R. O., Kennedy-Bowdoin, T., Eastwood, M., Martin, R.
 830 E., Anderson, C., and Field, C. B.: Carnegie Airborne Observatory-2: Increasing science data
 831 dimensionality via high-fidelity multi-sensor fusion, *Remote Sens. Environ.*, 124, 454-465,
 832 10.1016/j.rse.2012.06.012, 2012.
- 833 Asner, G. P., Knapp, D. E., Martin, R. E., Tupayachi, R., Anderson, C. B., Mascaro, J., Sinca, F.,
 834 Chadwick, K. D., Higgins, M., Farfan, W., Llactayo, W., and Silman, M. R.: Targeted carbon
 835 conservation at national scales with high-resolution monitoring, *P. Natl. Acad. Sci. USA*, 111,
 836 E5016-E5022, 10.1073/pnas.1419550111, 2014.
- 837 Barke, R., and Lamb, S.: Late Cenozoic uplift of the Eastern Cordillera, Bolivian Andes, *Earth Planet*
 838 *Sc. Lett.*, 249, 350-367, 10.1016/j.epsl.2006.07.012, 2006.
- 839 Bilderback, E. L., Pettinga, J. R., Litchfield, N. J., Quigley, M., Marden, M., Roering, J. J., and Palmer, A.
 840 S.: Hillslope response to climate-modulated river incision in the Waipaoa catchment, East
 841 Coast North Island, New Zealand, *Geol. Soc. Am. Bull.*, 127, 131-148, 10.1130/B31015.1,
 842 2015.
- 843 Blodgett, T. A., and Isacks, B. L.: Landslide erosion rate in the eastern cordillera of northern Bolivia,
 844 *Earth Interact.*, 11, 1-30, 10.1175/2007EI222.1, 2007.
- 845 Bookhagen, B.: High resolution spatiotemporal distribution of rainfall seasonality and extreme
 846 events based on a 12-year TRMM time series
 847 <http://www.geog.ucsb.edu/~bodo/TRMM/index.php>, (accessed 06/06/2013), 2013.
- 848 Bouchez, J., Galy, V., Hilton, R. G., Gaillardet, J., Moreira-Turcq, P., Pérez, M. A., France-Lanord, C.,
 849 and Maurice, L.: Source, transport and fluxes of Amazon River particulate organic carbon:
 850 insights from river sediment depth-profiles, *Geochim. Cosmochim. Ac.*, 133, 280-298,
 851 10.1016/j.gca.2014.02.032, 2014.
- 852 Brozović, N., Burbank, D. W., and Meigs, A. J.: Climatic limits on landscape development in the
 853 Northwestern Himalaya, *Science*, 276, 571-574, 10.1126/science.276.5312.571, 1997.
- 854 Burbank, D. W., Leland, J., Fielding, E., Anderson, R. S., Brozovic, N., Reid, M. R., and Duncan, C.:
 855 Bedrock incision, rock uplift and threshold hillslopes in the northwestern Himalayas, *Nature*,
 856 379, 505-510, 10.1038/379505a0, 1996.
- 857 Bussmann, R. W., Wilcke, W., and Richter, M.: Landslides as important disturbance regimes - Causes
 858 and regeneration, in: *Gradients in a tropical mountain ecosystem of Ecuador*, edited by:
 859 Beck, E., Bendix, J., Kottke, I., Makeschin, F., and Mosandl, R., *Ecological Studies*, 198,
 860 Springer-Verlag, Berlin Heidelberg, Germany, 321-330, 2008.
- 861 Cabrera, J., Sébrier, M., and Mercier, J. L.: Plio-Quaternary geodynamic evolution of a segment of the
 862 Peruvian Andean Cordillera located above the change in the subduction geometry: The
 863 Cuzco region, *Tectonophysics*, 190, 331-362, 10.1016/0040-1951(91)90437-W, 1991.
- 864 Carlotto Caillaux, V. S., Rodriguez, G., Fernando, W., Roque, C., Dionicio, J., and Chávez, R.: *Geología*
 865 *de los cuadrángulos de Urubamba y Calca*, Instituto Geológica Nacional, Lima, Peru, 1996.
- 866 Casagli, N., Dapporto, S., Ibsen, M. L., Tofani, V., and Vannocci, P.: Analysis of the landslide triggering
 867 mechanism during the storm of 20th–21st November 2000, in *Northern Tuscany, Landslides*,
 868 3, 13-21, 10.1007/s10346-005-0007-y, 2006.
- 869 Clark, K. E., Hilton, R. G., West, A. J., Malhi, Y., Gröcke, D. R., Bryant, C. L., Ascough, P. L., Robles
 870 Caceres, A., and New, M.: New views on “old” carbon in the Amazon River: Insight from the

871 source of organic carbon eroded from the Peruvian Andes, *Geochem. Geophys. Geosy.*, 14,
872 1644-1659, 10.1002/ggge.20122, 2013.

873 Clark, K. E., Torres, M. A., West, A. J., Hilton, R. G., New, M., Horwath, A. B., Fisher, J. B., Rapp, J. M.,
874 Robles Caceres, A., and Malhi, Y.: The hydrological regime of a forested tropical Andean
875 catchment, *Hydrol. Earth Syst. Sci.*, 18, 5377-5397, 10.5194/hess-18-5377-2014, 2014.

876 Clark, M. K., Royden, L. H., Whipple, K. X., Burchfiel, B. C., Zhang, X., and Tang, W.: Use of a regional,
877 relict landscape to measure vertical deformation of the eastern Tibetan Plateau, *J. Geophys.*
878 *Res.-Earth*, 111, 1-23, 10.1029/2005JF000294, 2006.

879 Connell, J. H.: Diversity in tropical rain forests and coral reefs, *Science*, 199, 1302-1310,
880 10.1126/science.199.4335.1302, 1978.

881 Consbio: Ecosistemas Terrestres de Peru (Data Basin Dataset) for ArcGIS, Covallis, Oregon, USA,
882 2011.

883 Crosby, B. T., Whipple, K. X., Gasparini, N. M., and Wobus, C. W.: Formation of fluvial hanging
884 valleys: Theory and simulation, *J. Geophys. Res.-Earth*, 112, 1-20, 10.1029/2006JF000566,
885 2007.

886 Dadson, S. J., Hovius, N., Chen, H., Dade, W. B., Lin, J.-C., Hsu, M.-L., Lin, C.-W., Horng, M.-J., Chen, T.-
887 C., Milliman, J., and Stark, C. P.: Earthquake-triggered increase in sediment delivery from an
888 active mountain belt, *Geology*, 32, 733-736, 10.1130/G20639.1 2004.

889 Densmore, A. L., and Hovius, N.: Topographic fingerprints of bedrock landslides, *Geology*, 28, 371-
890 374, 10.1130/0091-7613(2000)28<371:TFOBL>2.0.CO;2 2000.

891 DiBiase, R. A., and Whipple, K. X.: The influence of erosion thresholds and runoff variability on the
892 relationships among topography, climate, and erosion rate, *J. Geophys. Res.-Earth*, 116, 1-
893 17, 10.1029/2011JF002095, 2011.

894 Dislich, C., and Huth, A.: Modelling the impact of shallow landslides on forest structure in tropical
895 montane forests, *Ecol. Model.*, 239, 40-53, 10.1016/j.ecolmodel.2012.04.016, 2012.

896 Dixon, R. K., Brown, S., Houghton, R., Solomon, A., Trexler, M., and Wisniewski, J.: Carbon pools and
897 flux of global forest ecosystems, *Science*, 263, 185-189, 1994.

898 Egholm, D. L., Knudsen, M. F., and Sandiford, M.: Lifespan of mountain ranges scaled by feedbacks
899 between landsliding and erosion by rivers, *Nature*, 498, 475-478, 10.1038/nature12218,
900 2013.

901 Ekström, G., and Stark, C. P.: Simple scaling of catastrophic landslide dynamics, *Science*, 339, 1416-
902 1419, 10.1126/science.1232887, 2013.

903 Engemann, K., Enquist, B. J., Sandel, B., Boyle, B., Jørgensen, P. M., Morueta-Holme, N., Peet, R. K.,
904 Violle, C., and Svenning, J.-C.: Limited sampling hampers "big data" estimation of species
905 richness in a tropical biodiversity hotspot, *Ecol. Evol.*, 5, 807-820, 10.1002/ece3.1405, 2015.

906 Espinoza, J. C., Chavez, S., Ronchail, J., Junquas, C., Takahashi, K., and Lavado, W.: Rainfall hotspots
907 over the southern tropical Andes: Spatial distribution, rainfall intensity, and relations with
908 large-scale atmospheric circulation, *Water Resour. Res.*, 51, 1-17, 10.1002/2014WR016273,
909 2015.

910 Eswaran, H., Van Den Berg, E., and Reich, P.: Organic Carbon in Soils of the World, *Soil Sci. Soc. Am.*
911 *J.*, 57, 192-194, 10.2136/sssaj1993.03615995005700010034x, 1993.

912 Farr, T. G., Rosen, P. A., Caro, E., Crippen, R., Duren, R., Hensley, S., Kobrick, M., Paller, M.,
913 Rodriguez, E., Roth, L., Seal, D., Shaffer, S., Shimada, J., Umland, J., Werner, M., Oskin, M.,
914 Burbank, D., and Alsdorf, D.: The Shuttle Radar Topography Mission, *Rev. Geophys.*, 45,
915 RG2004, 10.1029/2005RG000183, 2007.

916 Ferrier, K. L., Huppert, K. L., and Perron, J. T.: Climatic control of bedrock river incision, *Nature*, 496,
917 206-209, 10.1038/nature11982, 2013.

918 Gallen, S. F., Clark, M. K., and Godt, J. W.: Coseismic landslides reveal near-surface rock strength in a
919 high-relief tectonically active setting, *Geology*, 43, 70-70, 10.1130/G36080.1 2015.

920 Galy, V., Peucker-Ehrenbrink, B., and Eglinton, T.: Global carbon export from the terrestrial
921 biosphere controlled by erosion, *Nature*, 521, 204-207, 10.1038/nature14400, 2015.

922 Gasparini, N. M., and Whipple, K. X.: Diagnosing climatic and tectonic controls on topography:
923 Eastern flank of the northern Bolivian Andes, *Lithosphere*, 6, 230-250, 10.1130/l322.1, 2014.

924 Gibbon, A., Silman, M. R., Malhi, Y., Fisher, J. B., Meir, P., Zimmermann, M., Dargie, G. C., Farfan, W.
925 R., and Garcia, K. C.: Ecosystem carbon storage across the grassland-forest transition in the
926 high Andes of Manu National Park, Peru, *Ecosystems*, 13, 1097-1111, 10.1007/s10021-010-
927 9376-8, 2010.

928 Gilbert, G. K.: *Geology of the Henry Mountains*, Geology of the Henry Mountains, Washington, D.C.,
929 Report, i-160 pp., 1877.

930 Girardin, C. A. J., Malhi, Y., Aragao, L. E. O. C., Mamani, M., Huasco, W. H., Durand, L., Feeley, K. J.,
931 Rapp, J., Silva-Espejo, J. E., Silman, M., Salinas, N., and Whittaker, R. J.: Net primary
932 productivity allocation and cycling of carbon along a tropical forest elevational transect in
933 the Peruvian Andes, *Glob. Change Biol.*, 16, 3176-3192, 10.1111/j.1365-2486.2010.02235.x,
934 2010.

935 Girardin, C. A. J., Aragão, L. E. O. C., Malhi, Y., Huaraca Huasco, W., Metcalfe, D. B., Durand, L.,
936 Mamani, M., Silva-Espejo, J. E., and Whittaker, R. J.: Fine root dynamics along an elevational
937 gradient in tropical Amazonian and Andean forests, *Global Biogeochem. Cy.*, 27, 252-264,
938 10.1029/2011GB004082, 2013.

939 Girardin, C. A. J., Malhi, Y., Feeley, K. J., Rapp, J. M., Silman, M. R., Meir, P., Huaraca Huasco, W.,
940 Salinas, N., Mamani, M., Silva-Espejo, J. E., García Cabrera, K., Farfan Rios, W., Metcalfe, D.
941 B., Doughty, C. E., and Aragão, L. E. O. C.: Seasonality of above-ground net primary
942 productivity along an Andean altitudinal transect in Peru, *J. Trop. Ecol.*, 30, 503-519,
943 10.1017/S0266467414000443, 2014a.

944 Girardin, C. A. J., Silva-Espejo, J. E., Doughty, C. E., Huaraca Huasco, W., Metcalfe, D. B., Durand-Baca,
945 L., Marthews, T. R., Aragao, L. E. O. C., Farfan Rios, W., García Cabrera, K., Halladay, K.,
946 Fisher, J. B., Galiano-Cabrera, D. F., Huaraca-Quispe, L. P., Alzamora-Taype, I., Equiluz-Mora,
947 L., Salinas-Revilla, N., Silman, M., Meir, P., and Malhi, Y.: Productivity and carbon allocation
948 in a tropical montane cloud forest of the Peruvian Andes, *Plant Ecol. Divers.*, 7, 107-123,
949 10.1080/17550874.2013.820222, 2014b.

950 Glade, T.: Establishing the frequency and magnitude of landslide-triggering rainstorm events in New
951 Zealand, *Eng. Geol.*, 35, 160-174, 10.1007/s002540050302, 1998.

952 Gregory-Wodzicki, K. M.: Uplift history of the Central and Northern Andes: A review, *Geol. Soc. Am.*
953 *Bull.*, 112, 1091-1105, 10.1130/0016-7606(2000)112<1091:UHOTCA>2.0.CO;2 2000.

954 Gubbels, T. L., Isacks, B. L., and Farrar, E.: High-level surfaces, plateau uplift, and foreland
955 development, Bolivian central Andes, *Geology*, 21, 695-698, 10.1130/0091-
956 7613(1993)021<0695:hlsqua>2.3.co;2, 1993.

957 Gurdak, D. J., Aragao, L. E. O. C., Rozas-Dávila, A., Huaraca Huasco, W., García Cabrera, K., Doughty,
958 C. E., Farfan-Rios, W., Silva-Espejo, J. E., Metcalfe, D. B., Silman, M. R., and Malhi, Y.:
959 Assessing above-ground woody debris dynamics along a gradient of elevation in Amazonian
960 cloud forests in Peru: balancing above-ground inputs and respiration outputs, *Plant Ecol.*
961 *Divers.*, 7, 143-160, 10.1080/17550874.2013.818073, 2014.

962 Guzzetti, F., Peruccacci, S., Rossi, M., and Stark, C. P.: Rainfall thresholds for the initiation of
963 landslides in central and southern Europe, *Meteorol. Atmos. Phys.*, 98, 239-267,
964 10.1007/s00703-007-0262-7, 2007.

965 Halladay, K., Malhi, Y., and New, M.: Cloud frequency climatology at the Andes/Amazon transition: 1.
966 Seasonal and diurnal cycles, *J. Geophys. Res.*, 117, D23102, 10.1029/2012JD017770, 2012.

967 Hilton, R. G., Galy, A., and Hovius, N.: Riverine particulate organic carbon from an active mountain
968 belt: Importance of landslides, *Global Biogeochem. Cy.*, 22, BG1017,
969 10.1029/2006GB002905, 2008a.

970 Hilton, R. G., Galy, A., Hovius, N., Chen, M.-C., Horng, M.-J., and Chen, H.: Tropical-cyclone-driven
971 erosion of the terrestrial biosphere from mountains, *Nat Geosci*, 1, 759-762,
972 10.1038/ngeo333, 2008b.

973 Hilton, R. G., Meunier, P., Hovius, N., Bellingham, P. J., and Galy, A.: Landslide impact on organic
974 carbon cycling in a temperate montane forest, *Earth Surf. Proc. Land.*, 36, 1670-1679,
975 10.1002/esp.2191, 2011.

976 Hilton, R. G., Gaillardet, J., Calmels, D., and Birck, J.-L.: Geological respiration of a mountain belt
977 revealed by the trace element rhenium, *Earth Planet Sc. Lett.*, 403, 27-36,
978 10.1016/j.epsl.2014.06.021, 2014.

979 Horwath, A.: Epiphytic bryophytes as cloud forest indicators: Stable isotopes, biomass and diversity
980 along an altitudinal gradient in Peru, Doctor of Philosophy, Plant Sciences, University of
981 Cambridge, Cambridge, 260 pp., 2011.

982 Hovius, N., Stark, C. P., and Allen, P. A.: Sediment flux from a mountain belt derived by landslide
983 mapping, *Geology*, 25, 231-234, 10.1130/0091-7613(1997)025<0231:sffamb>2.3.co;2, 1997.

984 Hovius, N., Stark, C. P., Chu, H. T., and Lin, J. C.: Supply and removal of sediment in a landslide-
985 dominated mountain belt: Central Range, Taiwan, *J. Geol.*, 108, 73-89, 10.1086/314387,
986 2000.

987 Huaraca Huasco, W., Girardin, C. A. J., Doughty, C. E., Metcalfe, D. B., Baca, L. D., Silva-Espejo, J. E.,
988 Cabrera, D. G., Aragão, L. E. O., Davila, A. R., Marthews, T. R., Huaraca-Quispe, L. P.,
989 Alzamora-Taype, I., Eguiluz-Mora, L., Farfan-Rios, W., Cabrera, K. G., Halladay, K., Salinas-
990 Revilla, N., Silman, M., Meir, P., and Malhi, Y.: Seasonal production, allocation and cycling of
991 carbon in two mid-elevation tropical montane forest plots in the Peruvian Andes, *Plant Ecol.*
992 *Divers.*, 1-2, 125-142, 10.1080/17550874.2013.819042, 2014.

993 Hupp, C. R.: Seedling establishment on a landslide site, *Castanea*, 48, 89-98, 1983.

994 INGEMMET: GEOCATMIN - Geologia integrada por proyectos regionales, Lima, Peru, 2013.

995 Keefer, D. K.: The importance of earthquake-induced landslides to long-term slope erosion and
996 slope-failure hazards in seismically active regions, *Geomorphology*, 10, 265-284,
997 10.1016/0169-555X(94)90021-3, 1994.

998 Kessler, M.: Plant species richness and endemism during natural landslide succession in a perhumid
999 montane forest in the Bolivian Andes, *Ecotropica*, 5, 123-136, 1999.

1000 Lague, D., Hovius, N., and Davy, P.: Discharge, discharge variability, and the bedrock channel profile,
1001 *J. Geophys. Res.-Earth*, 110, 1-17, 10.1029/2004JF000259, 2005.

1002 Larsen, I. J., Montgomery, D. R., and Korup, O.: Landslide erosion controlled by hillslope material,
1003 *Nat. Geosci.*, 3, 247-251, 10.1038/ngeo776, 2010.

1004 Larsen, I. J., and Montgomery, D. R.: Landslide erosion coupled to tectonics and river incision, *Nat.*
1005 *Geosci.*, 5, 468-473, 10.1038/ngeo1479, 2012.

1006 Larsen, M. C., and Simon, A.: A rainfall intensity-duration threshold for landslides in a humid-tropical
1007 environment, Puerto Rico, *Geogr. Ann. A.*, 75, 13-23, 10.2307/521049, 1993.

1008 Li, G., West, A. J., Densmore, A. L., Jin, Z., Parker, R. N., and Hilton, R. G.: Seismic mountain building:
1009 Landslides associated with the 2008 Wenchuan earthquake in the context of a generalized
1010 model for earthquake volume balance, *Geochem. Geophys. Geosy.*, 15, 833-844,
1011 10.1002/2013GC005067, 2014.

1012 Lin, G.-W., Chen, H., Hovius, N., Horng, M.-J., Dadson, S., Meunier, P., and Lines, M.: Effects of
1013 earthquake and cyclone sequencing on landsliding and fluvial sediment transfer in a
1014 mountain catchment, *Earth Surf. Proc. Land.*, 33, 1354-1373, 10.1002/esp.1716, 2008.

1015 Lowman, L. E. L., and Barros, A. P.: Investigating links between climate and orography in the Central
1016 Andes: Coupling erosion and precipitation using a physical-statistical model, *J. Geophys.*
1017 *Res.-Earth*, 119, 1322-1353, 10.1002/2013JF002940, 2014.

1018 Malamud, B. D., Turcotte, D. L., Guzzetti, F., and Reichenbach, P.: Landslide inventories and their
1019 statistical properties, *Earth Surf. Proc. Land.*, 29, 687-711, 10.1002/esp.1064, 2004.

1020 Malhi, Y., Silman, M., Salinas, N., Bush, M., Meir, P., and Saatchi, S.: Introduction: Elevation gradients
1021 in the tropics: Laboratories for ecosystem ecology and global change research, *Glob. Change*
1022 *Biol.*, 16, 3171-3175, 10.1111/j.1365-2486.2010.02323.x, 2010.

1023 Marc, O., and Hovius, N.: Amalgamation in landslide maps: effects and automatic detection, *Nat.*
1024 *Hazards Earth Syst. Sci.*, 15, 723-733, 10.5194/nhess-15-723-2015, 2015.

1025 Marengo, J. A., Soares, W. R., Saulo, C., and Nicolini, M.: Climatology of the low-level jet east of the
1026 Andes as derived from the NCEP-NCAR reanalyses: Characteristics and temporal variability, *J.*
1027 *Climate*, 17, 2261-2280, 10.1175/1520-0442(2004)017<2261:COTLJE>2.0.CO;2, 2004.

1028 Marvin, D. C., Asner, G. P., Knapp, D. E., Anderson, C. B., Martin, R. E., Sinca, F., and Tupayachi, R.:
1029 Amazonian landscapes and the bias in field studies of forest structure and biomass, *P. Natl.*
1030 *Acad. Sci. USA*, 111, E5224-E5232, 10.1073/pnas.1412999111, 2014.

1031 Mendivil Echevarría, S., and Dávila Manrique, D.: *Geología de los cuadrángulos de Cuzco y Livitaca*,
1032 Instituto Geológica Nacional, Lima, Peru, 1994.

1033 METI/NASA: ASTER Global DEM product, NASA EOSDIS Land Processes DAAC USGS Earth Resources
1034 Observation and Science (EROS) Center Sioux Falls, South Dakota, USA, 2009.

1035 Meunier, P., Hovius, N., and Haines, J. A.: Topographic site effects and the location of earthquake
1036 induced landslides, *Earth Planet Sc. Lett.*, 275, 221-232, 10.1016/j.epsl.2008.07.020, 2008.

1037 Montgomery, D. R., and Buffington, J. M.: Channel-reach morphology in mountain drainage basins,
1038 *Geol. Soc. Am. Bull.*, 109, 596-611, 10.1130/0016-7606(1997)109<0596:CRMIMD>2.3.CO;2,
1039 1997.

1040 Montgomery, D. R.: Slope distributions, threshold hillslopes, and steady-state topography, *Am. J.*
1041 *Sci.*, 301, 432-454, 10.2475/ajs.301.4-5.432, 2001.

1042 Montgomery, D. R., and Brandon, M. T.: Topographic controls on erosion rates in tectonically active
1043 mountain ranges, *Earth Planet Sc. Lett.*, 201, 481-489, 10.1016/S0012-821X(02)00725-2,
1044 2002.

1045 Moon, S., Chamberlain, C. P., Blisniuk, K., Levine, D. H., Rood, D. H., and Hilley, G. E.: Climatic control
1046 of denudation in the deglaciated landscape of the Washington Cascades, *Nat. Geosci.*, 4,
1047 469-473, 10.1038/ngeo1159, 2011.

1048 Oskin, M., and Burbank, D. W.: Alpine landscape evolution dominated by cirque retreat, *Geology*, 33,
1049 933-936, 10.1130/G21957.1, 2005.

1050 Peltzer, D. A., Wardle, D. A., Allison, V. J., Baisden, W. T., Bardgett, R. D., Chadwick, O. A., Condon, L.
1051 M., Parfitt, R. L., Porder, S., and Richardson, S. J.: Understanding ecosystem retrogression,
1052 *Ecol. Mongr.*, 80, 509-529, 10.1890/09-1552.1, 2010.

1053 Pepin, E., Guyot, J. L., Armijos, E., Bazan, H., Fraizy, P., Moquet, J. S., Noriega, L., Lavado, W.,
1054 Pombosa, R., and Vauchel, P.: Climatic control on eastern Andean denudation rates (Central
1055 Cordillera from Ecuador to Bolivia), *J. S. Am. Earth Sci.*, 44, 85-93,
1056 10.1016/j.jsames.2012.12.010, 2013.

1057 Ponton, C., West, A. J., Feakins, S. J., and Galy, V.: Leaf wax biomarkers in transit record river
1058 catchment composition, *Geophys. Res. Lett.*, 41, 6420-6427, 10.1002/2014GL061328, 2014.

1059 Quesada, C. A., Lloyd, J., Schwarz, M., Patiño, S., Baker, T. R., Czimczik, C., Fyllas, N. M., Martinelli, L.,
1060 Nardoto, G. B., Schmerler, J., Santos, A. J. B., Hodnett, M. G., Herrera, R., Luizão, F. J., Arneith,
1061 A., Lloyd, G., Dezzio, N., Hilke, I., Kuhlmann, I., Raessler, M., Brand, W. A., Geilmann, H.,
1062 Moraes Filho, J. O., Carvalho, F. P., Araujo Filho, R. N., Chaves, J. E., Cruz Junior, O. F.,
1063 Pimentel, T. P., and Paiva, R.: Variations in chemical and physical properties of Amazon
1064 forest soils in relation to their genesis, *Biogeosciences*, 5, 1515 - 1541, 10.5194/bg-7-1515-
1065 2010, 2010.

1066 Raich, J. W., Russell, A. E., Kitayama, K., Parton, W. J., and Vitousek, P. M.: Temperature influences
1067 carbon accumulation in moist tropical forests, *Ecology*, 87, 76-87, 10.1890/05-0023, 2006.

1068 Ramos Scharrón, C. E., Castellanos, E. J., and Restrepo, C.: The transfer of modern organic carbon by
1069 landslide activity in tropical montane ecosystems, *J. Geophys. Res.-Biogeo.*, 117, G03016,
1070 10.1029/2011JG001838, 2012.

1071 Rao, Y.: Variation in plant carbon and nitrogen isotopes along an altitudinal gradient in the Peruvian
1072 Andes, *B.Sc.*, Department of Earth Sciences, Durham University, Durham, 60 pp., 2011.

- 1073 Restrepo, C., Vitousek, P., and Neville, P.: Landslides significantly alter land cover and the
1074 distribution of biomass: an example from the Ninole ridges of Hawai'i, *Plant Ecol.*, 166, 131-
1075 143, 10.1023/A:1023225419111, 2003.
- 1076 Restrepo, C., and Alvarez, N.: Landslides and their contribution to land-cover change in the
1077 mountains of Mexico and Central America, *Biotropica*, 38, 446-457, 10.1111/j.1744-
1078 7429.2006.00178.x, 2006.
- 1079 Restrepo, C., Walker, L. R., Shiels, A. B., Bussmann, R., Claessens, L., Fisch, S., Lozano, P., Negi, G.,
1080 Paolini, L., and Poveda, G.: Landsliding and its multiscale influence on mountainscapes,
1081 *Bioscience*, 59, 685-698, 10.1525/bio.2009.59.8.10, 2009.
- 1082 Roering, J. J., Kirchner, J. W., and Dietrich, W. E.: Characterizing structural and lithologic controls on
1083 deep-seated landsliding: Implications for topographic relief and landscape evolution in the
1084 Oregon Coast Range, USA, *Geol. Soc. Am. Bull.*, 117, 654-668, 10.1130/B25567.1, 2005.
- 1085 Roering, J. J., Mackey, B. H., Handwerger, A. L., Booth, A. M., Schmidt, D. A., Bennett, G. L., and
1086 Cerovski-Darriau, C.: Beyond the angle of repose: A review and synthesis of landslide
1087 processes in response to rapid uplift, Eel River, Northern California, *Geomorphology*, 236,
1088 109-131, 10.1016/j.geomorph.2015.02.013, 2015.
- 1089 Rohrmann, A., Strecker, M. R., Bookhagen, B., Mulch, A., Sachse, D., Pingel, H., Alonso, R. N.,
1090 Schildgen, T. F., and Montero, C.: Can stable isotopes ride out the storms? The role of
1091 convection for water isotopes in models, records, and paleoaltimetry studies in the central
1092 Andes, *Earth Planet Sc. Lett.*, 407, 187-195, 10.1016/j.epsl.2014.09.021, 2014.
- 1093 Saatchi, S. S., Houghton, R. A., Dos Santos Alvalá, R. C., Soares, J. V., and Yu, Y.: Distribution of
1094 aboveground live biomass in the Amazon basin, *Glob. Change Biol.*, 13, 816-837,
1095 10.1111/j.1365-2486.2007.01323.x, 2007.
- 1096 Saatchi, S. S., Harris, N. L., Brown, S., Lefsky, M., Mitchard, E. T., Salas, W., Zutta, B. R., Buermann,
1097 W., Lewis, S. L., and Hagen, S.: Benchmark map of forest carbon stocks in tropical regions
1098 across three continents, *P. Natl. Acad. Sci. USA*, 108, 9899-9904, 10.1073/pnas.1019576108,
1099 2011.
- 1100 Safran, E. B., Bierman, P. R., Aalto, R., Dunne, T., Whipple, K. X., and Caffee, M.: Erosion rates driven
1101 by channel network incision in the Bolivian Andes, *Earth Surf. Proc. Land.*, 30, 1007-1024,
1102 10.1002/esp.1259, 2005.
- 1103 Salazar, L., Homeier, J., Kessler, M., Abrahamczyk, S., Lehnert, M., Krömer, T., and Kluge, J.: Diversity
1104 patterns of ferns along elevational gradients in Andean tropical forests, *Plant Ecol. Divers.*, 8,
1105 13-24, 10.1080/17550874.2013.843036, 2015.
- 1106 Schmidt, K. M., and Montgomery, D. R.: Limits to relief, *Science*, 270, 617-620,
1107 10.1126/science.270.5236.617, 1995.
- 1108 Sébrier, M., Mercier, J. L., Mégard, F., Laubacher, G., and Carey-Gailhardis, E.: Quaternary normal
1109 and reverse faulting and the state of stress in the central Andes of south Peru, *Tectonics*, 4,
1110 739-780, 10.1029/TC004i007p00739, 1985.
- 1111 Selby, M.: *Hillslope materials and processes*, Oxford University Press, Oxford, UK, 289 pp., 1993.
- 1112 Stallard, R. F.: *River chemistry, geology, geomorphology, and soils in the Amazon and Orinoco Basins,*
1113 *The chemistry of weathering*, Rodez, France, 293-316, 1985.
- 1114 Stallard, R. F.: *Terrestrial sedimentation and the carbon cycle: Coupling weathering and erosion to*
1115 *carbon burial*, *Global Biogeochem. Cy.*, 12, 231-257, 10.1029/98gb00741, 1998.
- 1116 Stark, C. P., and Hovius, N.: The characterization of landslide size distributions, *Geophys. Res. Lett.*,
1117 28, 1091-1094, 10.1029/2000GL008527, 2001.
- 1118 Stock, J., and Dietrich, W. E.: Valley incision by debris flows: Evidence of a topographic signature,
1119 *Water Resour. Res.*, 39, 1-24, 10.1029/2001WR001057, 2003.
- 1120 Stoyan, R.: *Aktivität, Ursachen und Klassifikation der Rutschungen in San Francisco/Süd Ecuador,*
1121 *Diploma*, University of Erlangen-Nuremberg, Erlangen, Germany, 2000.

1122 Strecker, M. R., Alonso, R. N., Bookhagen, B., Carrapa, B., Hilley, G. E., Sobel, E. R., and Trauth, M. H.:
1123 Tectonics and climate of the Southern Central Andes, *Annu. Rev. Earth Pl. Sc.*, 35, 747-787,
1124 10.1146/annurev.earth.35.031306.140158, 2007.

1125 Tavera, H., and Buforn, E.: Source mechanism of earthquakes in Perú, *J. Seismol.*, 5, 519-540,
1126 10.1023/A:1012027430555, 2001.

1127 Terzaghi, K.: Mechanism of landslides, Harvard University, Department of Engineering, Cambridge,
1128 Massachusetts, USA, 41 pp., 1951.

1129 USGS: Earthquakes v3.6, 2013-07-02, USGS, <http://earthquake.usgs.gov/earthquakes/map/>, access:
1130 02/07/2013, 2013a.

1131 USGS: Landsat Processing Details, United States Geological Survey, U.S. Department of the Interior,
1132 http://landsat.usgs.gov/Landsat_Processing_Details.php, access: 16/7/2013, 2013b.

1133 Vargas Vilchez, L., and Hipolito Romero, A.: Geología de los cuadrángulos de Río Piquén, Pilcopata y
1134 Chontachaca. Hojas: 25-t, 26-t y 27-t, Instituto Geológica Nacional, Lima, Peru, 1998.

1135 Walker, L. R., Zarin, D. J., Fetcher, N., Myster, R. W., and Johnson, A. H.: Ecosystem development and
1136 plant succession on landslides in the Caribbean, *Biotropica*, 28, 566-576, 10.2307/2389097,
1137 1996.

1138 Walker, L. R., Shiels, A. B., Bellingham, P. J., Sparrow, A. D., Fetcher, N., Landau, F. H., and Lodge, D.
1139 J.: Changes in abiotic influences on seed plants and ferns during 18 years of primary
1140 succession on Puerto Rican landslides, *J. Ecol.*, 101, 650-661, 10.1111/1365-2745.12071,
1141 2013.

1142 Wang, G., and Sassa, K.: Pore-pressure generation and movement of rainfall-induced landslides:
1143 effects of grain size and fine-particle content, *Eng. Geol.*, 69, 109-125, 10.1016/S0013-
1144 7952(02)00268-5, 2003.

1145 Wang, J., Jin, Z., Hilton, R. G., Zhang, F., Densmore, A. L., Li, G., and West, A. J.: Controls on fluvial
1146 evacuation of sediment from earthquake-triggered landslides, *Geology*, 43, 115-118,
1147 10.1130/G36157.1, 2015.

1148 West, A. J., Lin, C. W., Lin, T. C., Hilton, R. G., Liu, S. H., Chang, C. T., Lin, K. C., Galy, A., Sparkes, R. B.,
1149 and Hovius, N.: Mobilization and transport of coarse woody debris to the oceans triggered
1150 by an extreme tropical storm, *Limnol. Oceanogr.*, 56, 77-85, 10.4319/lo.2011.56.1.0077,
1151 2011.

1152 Whipple, K. X.: Fluvial landscape response time: How plausible is steady-state denudation?, *Am. J.*
1153 *Sci.*, 301, 313-325, 10.2475/ajs.301.4-5.313, 2001.

1154 Whipple, K. X.: Bedrock rivers and the geomorphology of active orogens, *Annu. Rev. Earth Pl. Sc.*, 32,
1155 151-185, 10.1146/annurev.earth.32.101802.120356, 2004.

1156 Whipple, K. X., and Gasparini, N. M.: Tectonic control of topography, rainfall patterns, and erosion
1157 during rapid post-12 Ma uplift of the Bolivian Andes, *Lithosphere*, 6, 251-268,
1158 10.1130/l325.1, 2014.

1159 Wittmann, H., von Blanckenburg, F., Guyot, J. L., Maurice, L., and Kubik, P.: From source to sink:
1160 Preserving the cosmogenic ¹⁰Be-derived denudation rate signal of the Bolivian Andes in
1161 sediment of the Beni and Mamoré foreland basins, *Earth Planet Sc. Lett.*, 288, 463-474,
1162 10.1016/j.epsl.2009.10.008, 2009.

1163 Wohl, E., and Ogden, F. L.: Organic carbon export in the form of wood during an extreme tropical
1164 storm, Upper Rio Chagres, Panama, *Earth Surf. Proc. Land.*, 38, 1407-1416,
1165 10.1002/esp.3389, 2013.

1166 Wolman, M. G., and Miller, J. P.: Magnitude and frequency of forces in geomorphic processes, *J.*
1167 *Geol.*, 68, 54-74, 1960.

1168 Yang, R., Willett, S. D., and Goren, L.: In situ low-relief landscape formation as a result of river
1169 network disruption, *Nature*, 520, 526-529, 10.1038/nature14354, 2015.

1170 Yoo, K., Amundson, R., Heimsath, A. M., and Dietrich, W. E.: Erosion of upland hillslope soil organic
1171 carbon: Coupling field measurements with a sediment transport model, *Global Biogeochem.*
1172 *Cy.*, 19, GB3003, 10.1029/2004GB002271, 2005.

1173 Zhang, W., and Montgomery, D. R.: Digital elevation model grid size, landscape representation,
1174 Water Resour. Res., 30, 1019-1028, 1994.

1175 Zimmermann, M., Meir, P., Bird, M. I., Malhi, Y., and Ccahuana, A. J. Q.: Climate dependence of
1176 heterotrophic soil respiration from a soil-translocation experiment along a 3000 m tropical
1177 forest altitudinal gradient, Eur. J. Soil Sci., 60, 895-906, 10.1111/j.1365-2389.2009.01175.x,
1178 2009.

1179

1180

1181

Table 1: Regressions for basin wide carbon stocks (tC km⁻²) for the Kosñipata Valley

Equation	Number of plots	R ²	P	Source of data
Soil = 4.01±4.64 x Elevation + 16665.22±11753.06	11 (with 6 to 51 subplots)	0.08	0.19	This study
AGLB = -1.16±0.65 x Elevation + 8553.71±1644.36	13	0.22	0.10	This study
BGLB = -0.22±0.13 x Elevation + 2237.09±280.18	6	0.43	0.16	(Girardin et al., 2010)

AGLB = Above ground living biomass (includes tree stems)
 BGLB = Below ground living biomass (includes fine and coarse roots)
 Regressions used to gain a general understanding of C stocks with elevation and significance of the relationship with elevation is not relevant.

1182

1183

1184

Table 2: Valley-wide landslide stripped organic carbon ($\text{tC km}^{-2} \text{yr}^{-1}$).

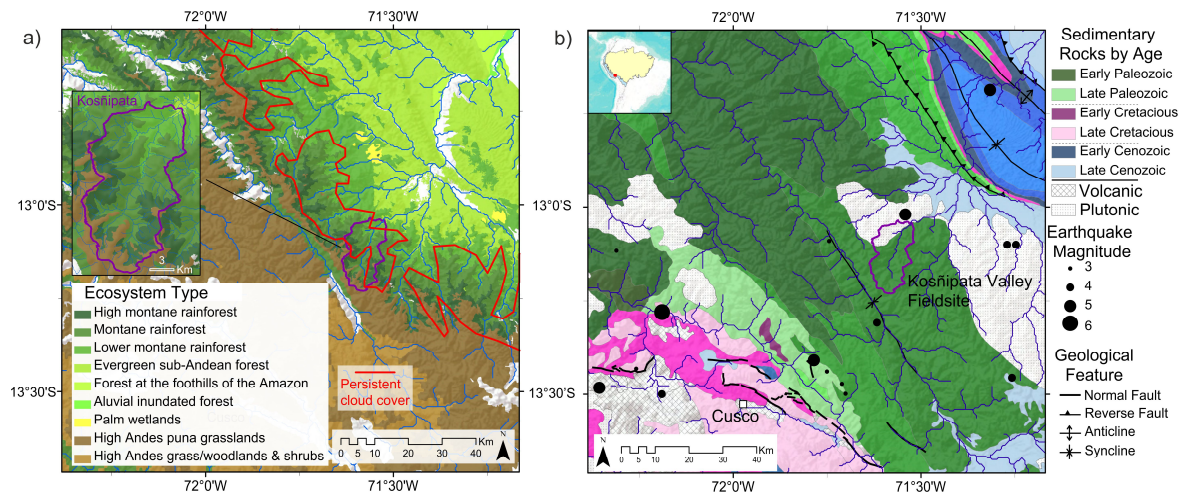
	1988 to 2012	Without 2010	2010
Total	<u>25.8 ± 3.6</u>	<u>19.1 ± 3.0</u>	<u>6.8 ± 1.2</u>
Soil	<u>20.1 ± 3.5</u>	<u>15.1 ± 2.9</u>	<u>5.0 ± 1.2</u>
Vegetation	<u>5.7 ± 0.8</u>	<u>4.0 ± 0.7</u>	<u>1.7 ± 0.2</u>

1185

1186

1187
1188

Figures

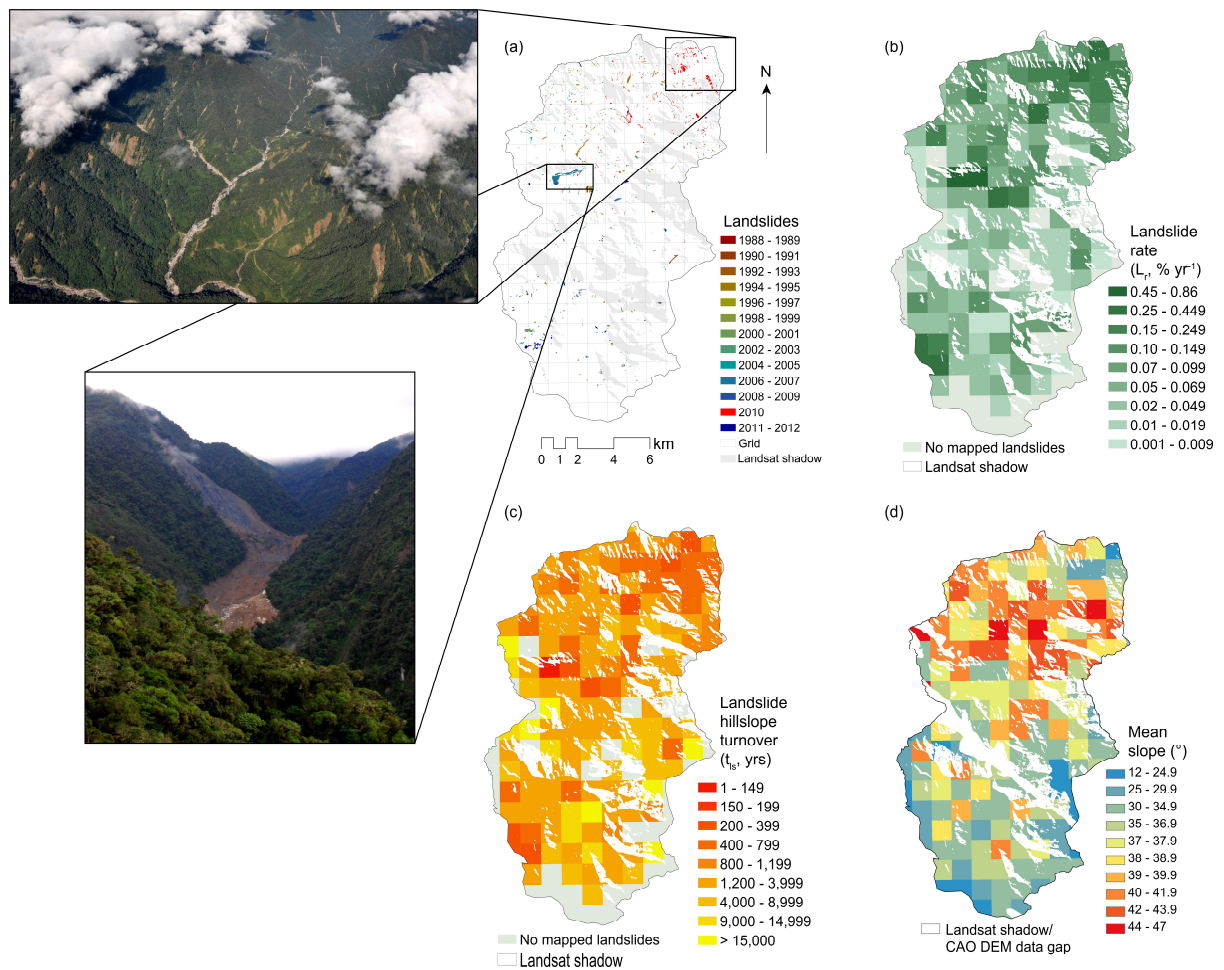


1189

1190 Figure 1: Maps of the study region. (a) Ecosystem types in the eastern Andes of Peru (Consbio, 2011).
1191 Bare areas are cities, agriculture, glaciers and riverbed, with the Kosñipata study catchment magnified
1192 in the inset. Areas delimited by red polygons are regions of > 75% annual cloud cover (Halladay et
1193 al., 2012). (b) Georectified geological map (INGEMMET, 2013; Vargas Vilchez and Hipolito
1194 Romero, 1998; Carlotto Caillaux et al., 1996; Mendivil Echevarría and Dávila Manrique, 1994);
1195 sedimentary rocks are on a scale ranging from dark to light colour within each era. Active faults
1196 (Cabrera et al., 1991; Sébrier et al., 1985) and documented earthquakes since 1975 (USGS, 2013a) are
1197 shown.

1198

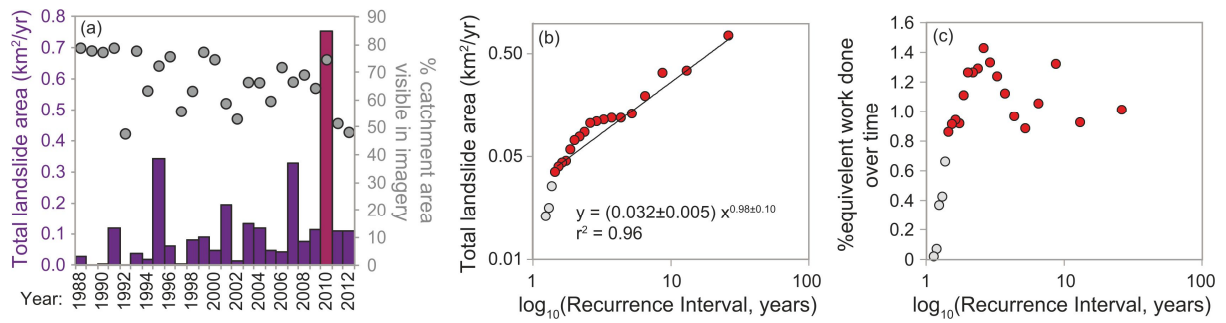
1199



1200

1201 Figure 2: (a) Landslides over the 25-year study period mapped from Landsat satellite images with
 1202 annual resolution, with Landsat topographic shadow regions in light grey. Photographs of the 2010
 1203 landslides (upper) taken by Gregory P. Asner from the Carnegie Airbone Observatory (CAO) in 2013,
 1204 and of the largest landslide in the study in 2007 (lower) taken by William Farfan-Rios from the
 1205 ground in 2011. (b) Landslide rates (R_{ls} , % yr⁻¹) calculated by 1 km² grid cell. (c) Hillslope turnover
 1206 (t_{ls} , yr) rates calculated as the time for landslides, at the current measured rate (R_{ls}), to impact 100% of
 1207 each cell area. (d) Catchment slopes calculated over a 1 km² grid for the visible portion of the study
 1208 area using the CAO DEM with 3m x 3m resolution.

1209

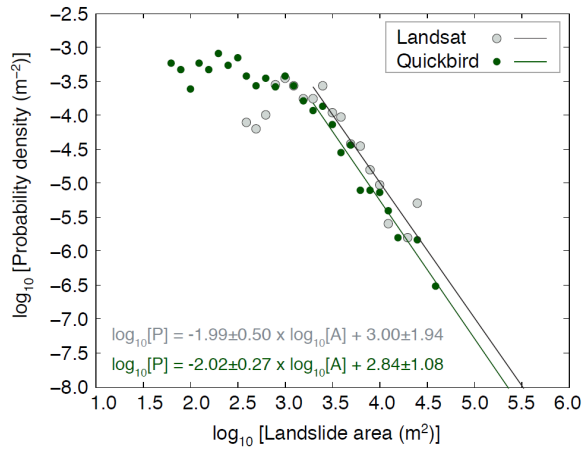


1210

1211 Figure 3: (a) Total area of landslides occurring each year in the dataset from this study, along with the
 1212 % area visible in the images used for each year. (b) Magnitude-frequency relationship for landslide
 1213 areas mapped in each year; red points are included in the regression while grey point are excluded
 1214 since these lowest-magnitude years depart from the linear relationship. (c) Estimate of integrated
 1215 work done by repeated events characteristic of given return times (see main text). Landslide area
 1216 mapped in 2010 was significantly higher than any other year because of landslides triggered by the
 1217 large storm in March 2010, but above a threshold magnitude, the integrated long-term landslide area
 1218 triggered by repeated events of smaller magnitude is similar to that done by larger, rarer events in this
 1219 dataset, as revealed by the similar % of equivalent work done for years across a wide range of inferred
 1220 recurrence interval.

1221

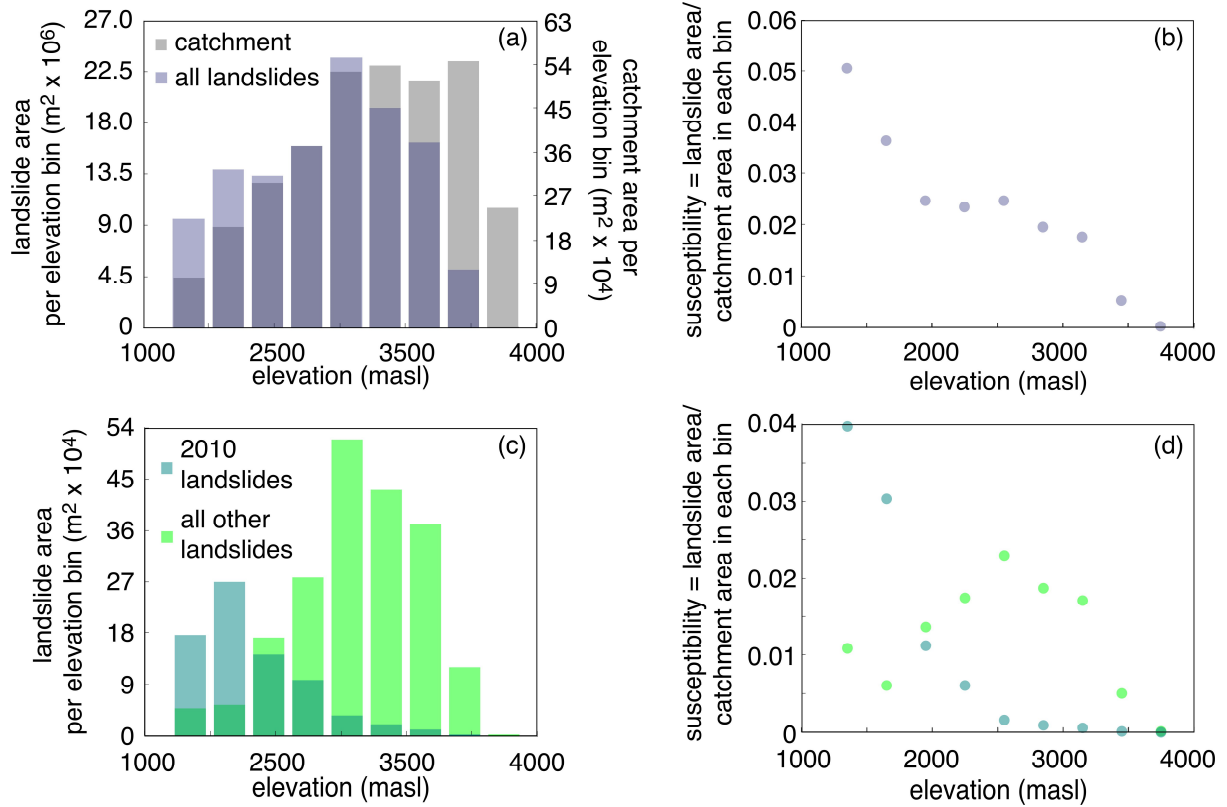
1222



1223

1224 Figure 4: Landslide area-frequency diagram for all landslides mapped from 1988 to 2005 in a region
 1225 of the Landsat image that overlapped with a Quickbird image from 2005, and for all landslides present
 1226 in the Landsat visible region of the Quickbird image. The higher frequency of small landslides in the
 1227 Quickbird inventory can be explained by the higher resolution of this image (2.4 m x 2.4 m, compared
 1228 to 30 m x 30 m for Landsat). The power law tails of the two inventories are similar.

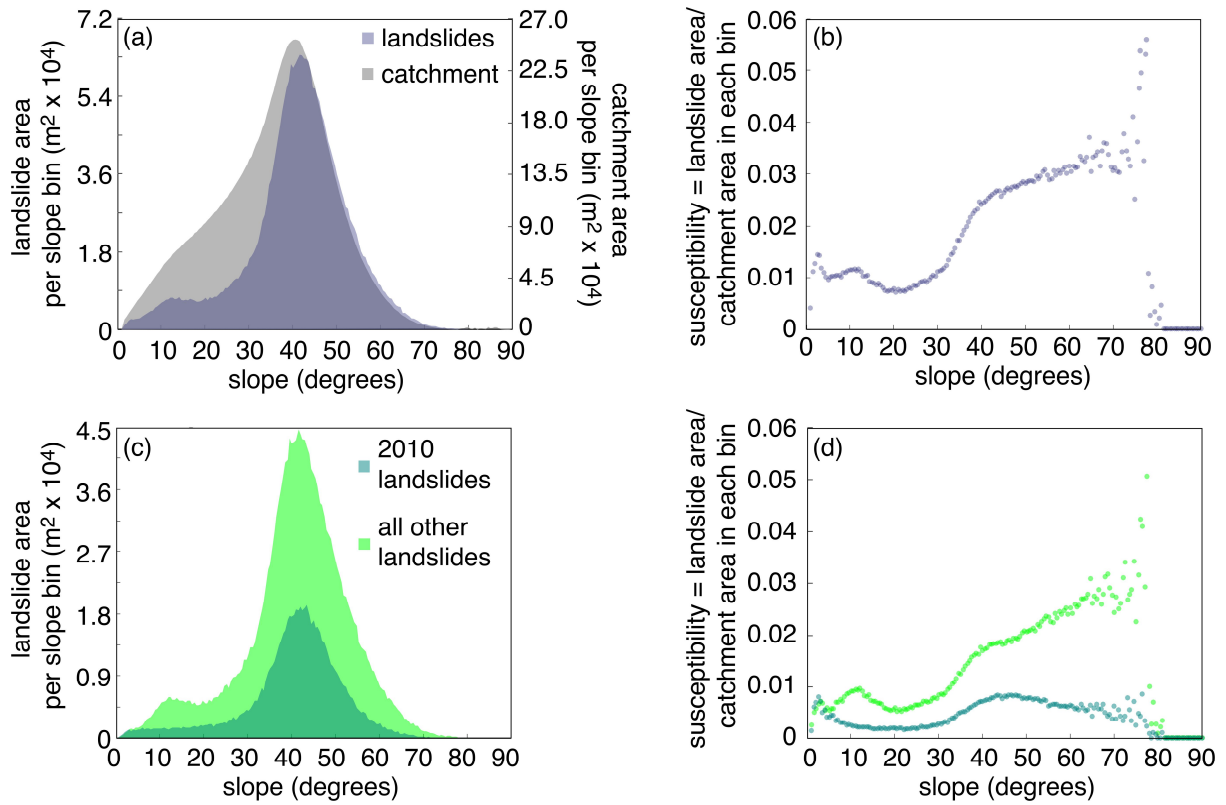
1229



1230

1231 Figure 5: Histograms of catchment and landslide areas by elevation bins of 300 m: (a) all landslides in
 1232 the 25-year dataset; (b,c) separating landslides occurring during 2010, associated with the large storm
 1233 in March 2010, from those in the rest of the dataset. (d) Corresponding calculation of
 1234 landslide susceptibility, calculated as the area of landslides within each bin divided by the total visible
 1235 area in the Landsat images used for mapping.

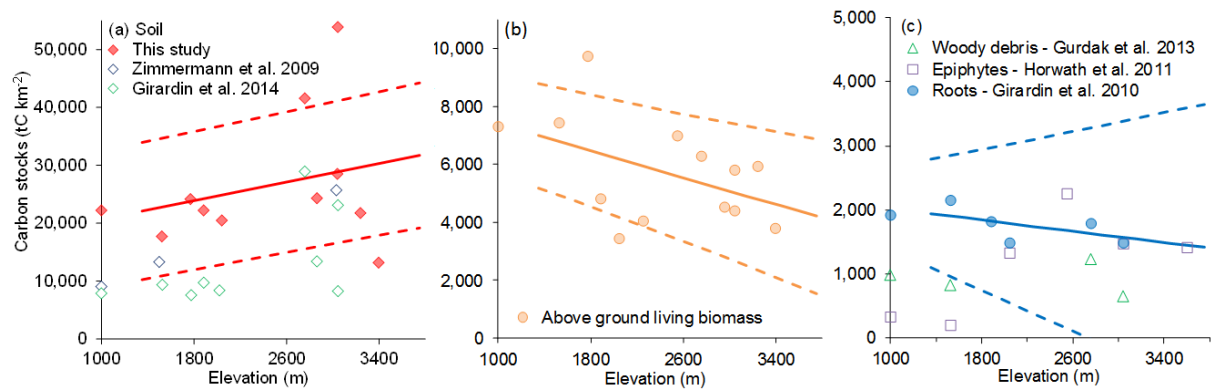
1236



1237

1238 Figure 6: Histograms of catchment and landslide areas by slope bins of 1° : (a) all landslides in the 25-
 1239 year dataset; (bc) separating landslides occurring during 2010, associated with the large storm in
 1240 March 2010, from those in the rest of the dataset. (eb) and (d) Corresponding calculation of landslide
 1241 susceptibility, calculated as the area of landslides within each bin divided by the total visible area in
 1242 the Landsat images used for mapping.

1243



1244

1245

1246

1247

1248

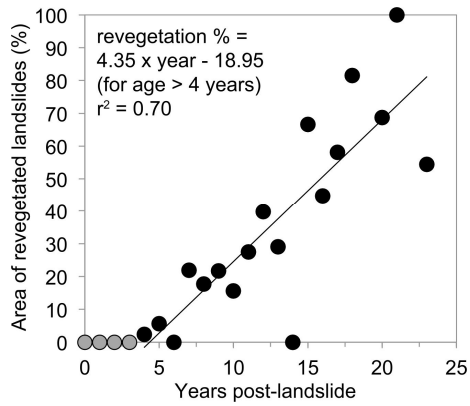
1249

1250

1251

1252

Figure 7: Soil and vegetation carbon stocks (tC km⁻²) as a function of elevation for the tropical montane forest of Kosñipata Valley, in the eastern Andes of Peru (Girardin et al., 2014a; Gurdak et al., 2014; Horwath, 2011; Girardin et al., 2010; Zimmermann et al., 2009). Linear regressions generated from available carbon stock data (tC km⁻²) from the Kosñipata Valley for a) soil carbon stocks (red diamonds only; see [Figure S1 and section 3.3.2. comparing the soil data](#) with other datasets), b) above ground living biomass, and c) [root biomass \(Table 1\)](#). c) [Woody debris](#), and epiphytes [are shown for reference](#).



1253

1254

Figure 8: Landslide revegetation time as percent area recovered by 2011, evaluated from a

1255

WorldView-2 pan-sharpened satellite image at 2 m x 2 m resolution. Each data point represents the

1256

landslides from a single year during the study period (black and grey circles; $n = 23$). Landslides

1257

occurring at least 4 years prior to 2011 (black circles) were used to calculate the best fit (area of

1258

revegetated landslides (%) = $4.351 \pm 0.719 \times \text{year of landslide origin prior to 2011} - 18.953 \pm 9.974$,

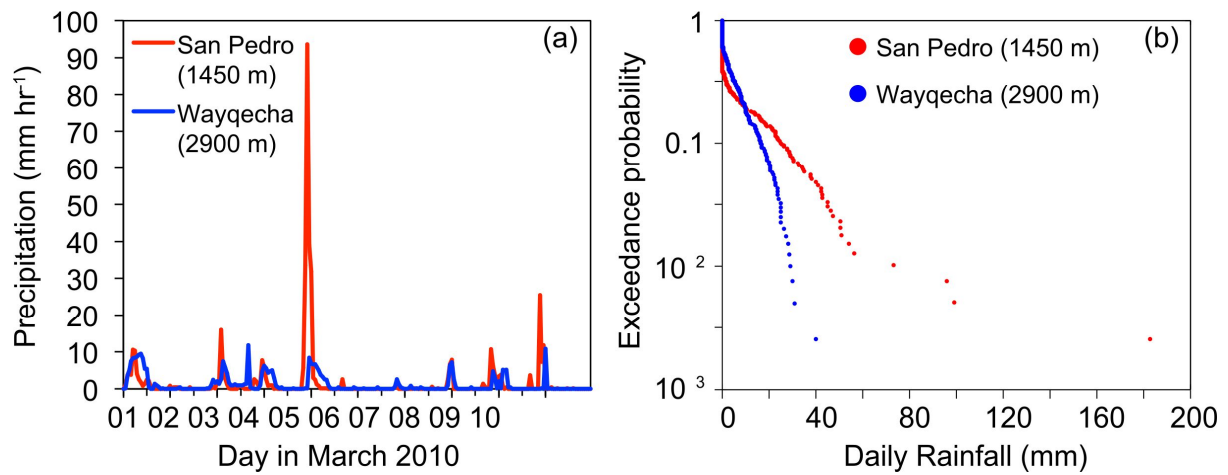
1259

where the mean estimated time for 100% revegetation of all the landslides of a given year is 27 ± 8 yrs

1260

($r^2 = 0.7$, $n = 18$, $p < 0.0001$).

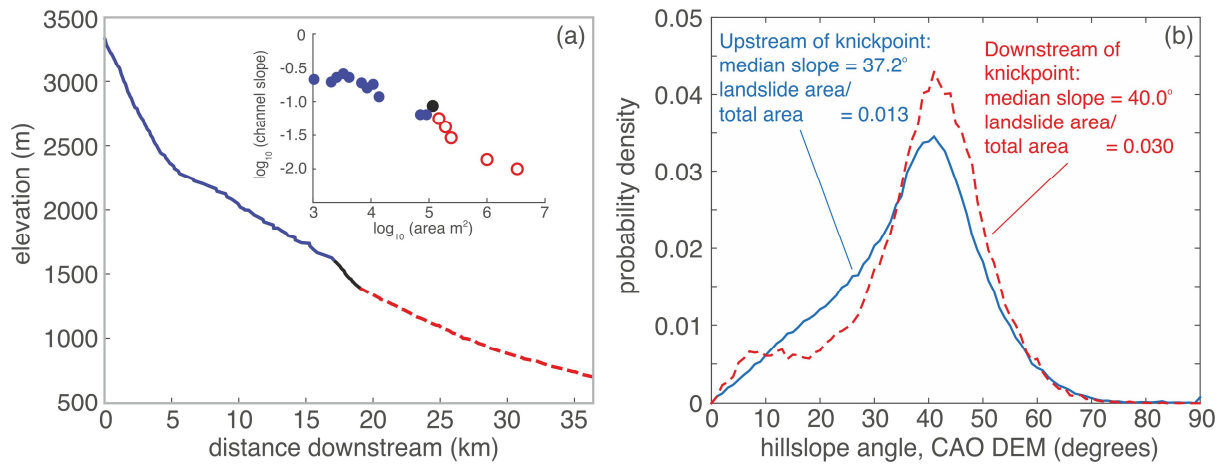
1261



1262

1263 Figure 9: (a) Precipitation during the March 2010 storm in the Kosñipata Valley at two stations, one at
 1264 high elevation (Wayqecha plot, 2900 m), where storm precipitation was low, and another at low
 1265 elevations (San Pedro, 1450 m) (Clark et al., 2014; ACCA, 2012), where precipitation was high and
 1266 where occurrence of storm-triggered landslides was also high (e.g., Fig. 5c). (b) Magnitude-frequency
 1267 analysis of precipitation over multiple years at the two stations shown in (a), demonstrating that the
 1268 low elevations in the Kosñipata study catchment are generally characterized by more low-frequency,
 1269 high-magnitude precipitation events.

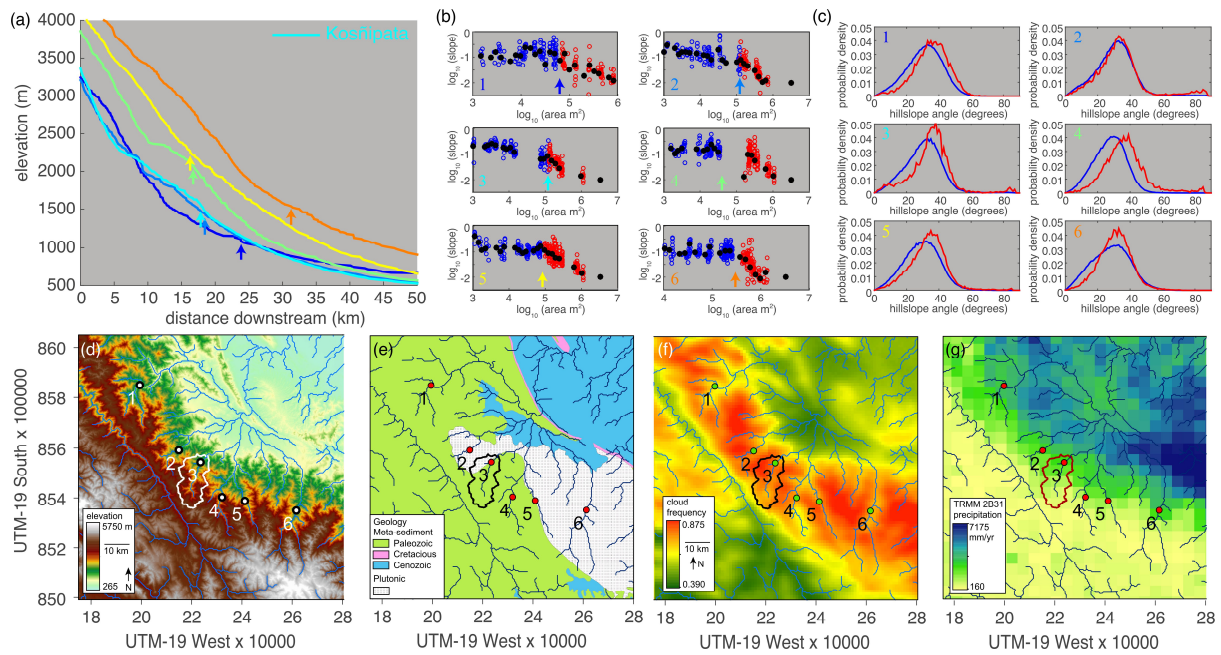
1270



1271

1272 Figure 10: (a) Longitudinal profile along the Kosñipata river channel, with a prominent vertical step
 1273 knickpoint corresponding to (inset) a transition in the plot between channel slope and upstream
 1274 contributing area, calculated following Moon et al. (2011). (b) Probability density of hillslope angles
 1275 (from 3 m x 3 m CAO DEM) upstream and downstream of the morphological transition in the
 1276 channel, along with median hillslope angles in each region and landslide susceptibility over the 25-
 1277 year study period.

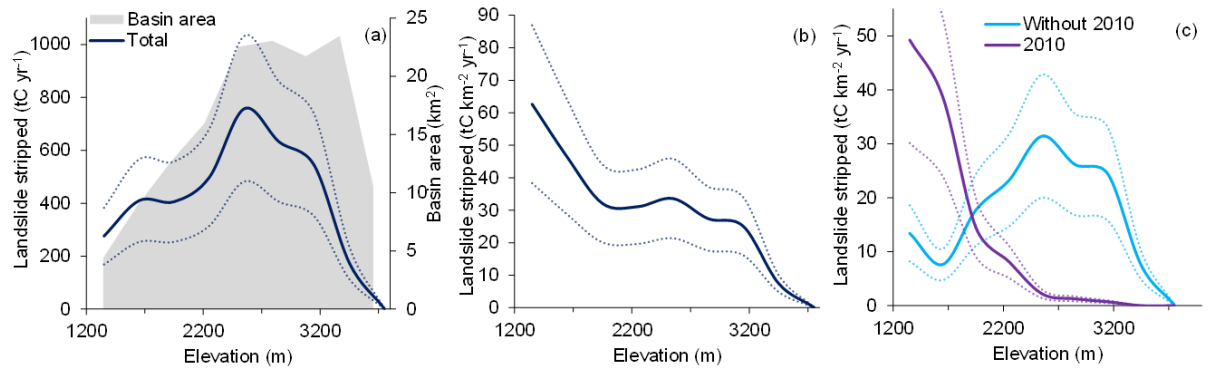
1278



1279

1280 Figure 11: (a-c) Analysis of river profiles analogous to those in Fig. 10 (shown here as River #3, in
 1281 cyan), for rivers throughout the Alto Madre de Dios region (d). In (b), data are binned by upstream
 1282 area and means are shown by black circles. Arrows in (a) refer to locations along the profile of
 1283 observed transition in the area-slope plots (b). In (c), hillslope angles (from STRM DEM) are grouped
 1284 by upstream (blue) and downstream (red) of this transition. Transition locations are displayed as dots
 1285 in (d-g), which show regional elevation (Farr et al., 2007) (d), geology (INGEMMET, 2013) (e),
 1286 Modis cloud frequency (Halladay et al., 2012) (f), and TRMM 2B31 annual precipitation (Bookhagen,
 1287 2013) (g).

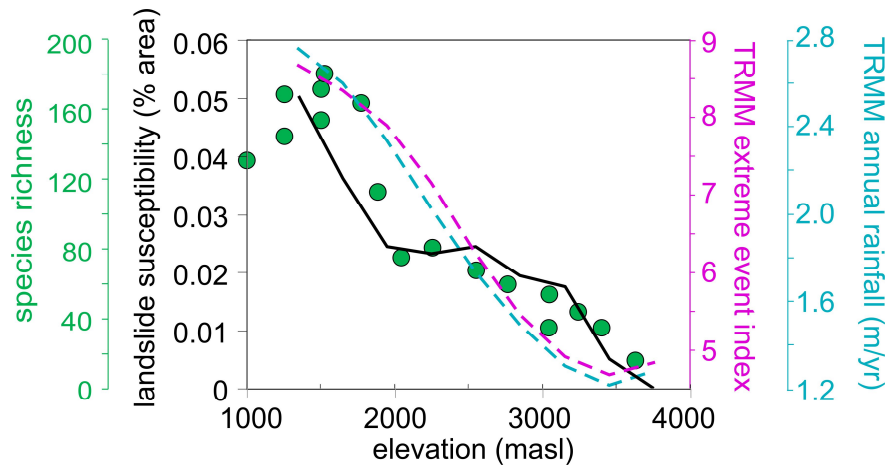
1288



1289

1290 Figure 12: (a) Total mobilisation of organic carbon by landslides (tC yr⁻¹) and (b) area-normalised
 1291 mobilisation of organic carbon (tC km⁻² yr⁻¹) over the altitudinal gradient divided into 300 m elevation
 1292 bins contributed by the sum of soil and vegetation (total, navy line), with errors as dotted lines.
 1293 Landslide susceptibility is highest at low elevations so the yield is highest there (b), but the total flux
 1294 due to landslides is dominated by mid-elevations that comprise the majority of basin area (a). (c)
 1295 Separation of landslide-mobilised organic carbon (tC km⁻² yr⁻¹) due to the 2010 rain storm event from
 1296 the remaining years as a function of elevation.

1297



1298

1299 Figure 13: Plots of landslide susceptibility, TRMM-based precipitation (both total annual precipitation
 1300 and TRMM extreme event index) (Bookhagen, 2013), and species richness, as a function of elevation
 1301 within the Kosñipata Valley. Note that absolute values of 2B31 TRMM annual precipitation are not
 1302 accurate without calibration to meteorological station data (cf. Clark et al. (2014)) but spatial patterns
 1303 may be representative. Climatology, landslide occurrence, and species richness all generally increase
 1304 from high to low elevations within the Kosñipata Valley, although landslide susceptibility and species
 1305 richness show a discontinuous trend with elevation while TRMM-based climatology is more
 1306 continuous.